ARMY RESEARCH LABORATORY

A Comparative Study of Nonlocal Density Functional Theory and *ab initio* Methods: The Potential Energy Surface of *sym*-Triazine Reactions

Sharmila V. Pai
Cary F. Chabalowski
Betsy M. Rice

ARL-TR-1217   October 1996

19961129 034

DTIC QUALITY INSPECTED 4

REPORT DOCUMENTATION PAGE

Public reporting burden for this collection of information is estimated to average 1 hour per response, including the time for reviewing instructions, searching existing data sources, gathering and maintaining the data needed, and completing and reviewing the collection of information. Send comments regarding this burden estimate or any other aspect of this collection of information, including suggestions for reducing this burden, to Washington Headquarters Services, Directorate for Information Operations and Reports, 1215 Jefferson Davis Highway, Suite 1204, Arlington, VA 22202-4302, and to the Office of Management and Budget, Paperwork Reduction Project(0704-0188), Washington, DC 20503.

1. AGENCY USE ONLY (Leave blank)	2. REPORT DATE	3. REPORT TYPE AND DATES COVERED
	October 1996	Final, Mar 95–Mar 96

4. TITLE AND SUBTITLE

A Comparative Study of Nonlocal Density Functional Theory and *ab initio* Methods: The Potential Energy Surface of *sym*-Triazine Reactions

5. FUNDING NUMBERS

PR: 1L161102AH43

6. AUTHOR(S)

Sharmila V. Pai, Cary F. Chabalowski, and Betsy M. Rice

7. PERFORMING ORGANIZATION NAME(S) AND ADDRESS(ES)

U.S. Army Research Laboratory
ATTN: AMSRL-WT-PC
Aberdeen Proving Ground, MD 21005-5066

8. PERFORMING ORGANIZATION REPORT NUMBER

ARL–TR–1217

9. SPONSORING/MONITORING AGENCY NAMES(S) AND ADDRESS(ES)

10. SPONSORING/MONITORING AGENCY REPORT NUMBER

11. SUPPLEMENTARY NOTES

12a. DISTRIBUTION/AVAILABILITY STATEMENT

Approved for public release; distribution is unlimited.

12b. DISTRIBUTION CODE

13. ABSTRACT (Maximum 200 words)

Critical points on the potential energy surface (PES) for *sym*-triazine ($C_3N_3H_3$) have been calculated using nonlocal density functional (NDFT) methods. The two decomposition mechanisms for *sym*-triazine investigated are a concerted triple dissociation of the *sym*-triazine ring to form the HCN products, where three-fold symmetry is maintained along the reaction path, and a step-wise decomposition mechanism involving formation of an intermediate dimer species. The NDFT structures, harmonic vibrational frequencies, and corresponding eigenvectors are compared with previously reported MP2 calculations. QCISD(T) energy refinements of the MP2 critical points are used for comparison with NDFT predictions. The NDFTs used are BP86; BLYP; B3LYP; and BPW91. Basis sets used are 6-31G**, 6-311++G**, and cc-pVTZ. The reaction endothermicity predicted by B3LYP and BPW91 are in closer agreement with experiment than the QCISD(T) and MP2 predictions using the largest basis set. B3LYP predictions are within 1.1 kcal/mol of experiment. BPW91, BP86, and BLYP frequencies agree most closely with experimental values for *sym*-triazine and HCN. DFT eigenvectors corresponding to vibrational modes for critical points on the PES compare well with MP2 predictions for most modes, indicating similarity in force fields and, therefore, atomic motion for the vibrations. Geometries predicted by all methods are in excellent agreement with experimental values for *sym*-triazine and HCN. All methods predict the concerted triple dissociation mechanism to be the low-energy decomposition pathway for *sym*-triazine.

14. SUBJECT TERMS

density functional theory, *sym*-triazine, potential energy surface, *ab initio*

15. NUMBER OF PAGES

42

16. PRICE CODE

17. SECURITY CLASSIFICATION OF REPORT	18. SECURITY CLASSIFICATION OF THIS PAGE	19. SECURITY CLASSIFICATION OF ABSTRACT	20. LIMITATION OF ABSTRACT
UNCLASSIFIED	UNCLASSIFIED	UNCLASSIFIED	UL

NSN 7540-01-280-5500

INTENTIONALLY LEFT BLANK.

ACKNOWLEDGMENTS

INTENTIONALLY LEFT BLANK.

TABLE OF CONTENTS

INTENTIONALLY LEFT BLANK.

LIST OF FIGURES

INTENTIONALLY LEFT BLANK.

LIST OF TABLES

INTENTIONALLY LEFT BLANK.

1. INTRODUCTION

Quantum chemistry is an invaluable tool in determining details of reaction mechanisms as well as in characterizing other properties of molecules (Schlegel 1987; Hehre et al. 1986). A proper description of the saddle point and the reaction path through quantum chemical calculations is of great importance because most details of these are inaccessible through experiment (Moeller 1934). Theory can give structures, characteristics, and energies of species along the entire reaction path through transition state and intrinsic reaction coordinate (IRC) calculations (Schlegel 1987; Hehre et al. 1986). A complete set of such information, however, requires computation of energies and energy derivatives of many points on the potential energy surface (PES). This can be accomplished at the Hartree Fock (HF) level for many molecules using modest computer resources. However, HF does not perform well in predicting reaction barriers and properties of structures with stretched bonds. Electron correlation must be introduced in order to improve the accuracy of these calculations. One of the least expensive of the *ab initio* electron correlation methods is second-order Moeller-Plesset (MP2) perturbation theory (Moeller 1934). However, post-HF treatments such as these scale as N^4 or greater, where N is the number of basis functions, effectively limiting the number of calculations, size of basis set, and size of the system studied. For systems in which the reaction path contains a multitude of transition states and minima and/or a large number of atoms, a complete determination of the reaction path becomes prohibitive.

Within the last decade, density functional theory (DFT) has offered a computationally less expensive yet reasonably accurate alternative to *ab initio* methods for including correlation corrections in calculating molecular properties such as geometries, frequencies, and energies (Hohenberg and Kohn 1964; Kohn and Sham 1965; Zeigler 1991; Labanowski and Andzelm 1991; Politzer and Seminario 1995). DFT can be applied to large polyatomic systems since the computational effort of density functional methods scales as N^3. Most of the successes of DFT have been in descriptions of stable molecules. The more sophisticated nonlocal DFT (NDFT) methods provide reaction energies and molecular properties that are typically better than the HF method and are closer to (and in some cases better than) the correlated methods (e.g., MP2) (Porezag and Pederson 1995; Broclawik et al. 1995; Jursic 1995; Deng and Zeigler 1995; Johnson et al. 1994; Deng, Branchadell, and Zeigler 1994; Sosa and Lee 1993; Fan and Zeigler 1992; Andzelm, Sosa,, and Eades 1993; Fan and Zeigler 1990). If DFT can correctly describe all of the important regions of the potential energy surfaces, such as transition states, stable intermediates, and points along reactions paths, detailed reaction mechanisms can be extracted for systems that are not accessible either through experiment or *ab initio* studies. Additionally, due to its modest computational requirements,

1

DFT appears to be the most promising quantum mechanical method to incorporate into dynamics simulations for the direct calculation of forces. If DFT can be shown to be reliable in describing chemical reactions, one of the main limitations of dynamics simulations (the use of analytic functions fitted to a limited set of data for the description of the interatomic interactions) will be removed for many cases. Therefore, it is imperative that studies such as those presented here compare the performance of DFT predictions of transition states and reaction paths with well-documented *ab initio* methods such as MP2 and QCISD(T) to determine both advantages and limitations of the methods.

There are a few studies that have applied DFT to transition-state and reaction-path predictions (Deng and Zeigler 1995; Johnson et al. 1994; Deng, Branchadell, and Zeigler 1994; Sosa and Lee 1993; Fan and Zeigler 1992; Andzelm, Sosa, and Eades 1993; Fan and Zeigler 1990; Baker et al. 1995). The performances of local and NDFT methods when compared to *ab initio* are not consistent. In some cases, DFT predictions of energy barriers are as good as *ab initio* or in closer agreement with experiment than *ab initio* (Deng and Zeigler 1995). In other cases, DFT fails completely in correctly describing reactions, such as predicting transition states as stable points (Johnson et al. 1994), or as nonexistent on the PES (Baker et al. 1995), or as having relative energies that are lower than the minimum to which it connects (Sosa and Lee 1993; Fan and Zeigler 1992). Also, local DFT has predicted minima on a PES that appear to be artifacts of the local density approximation, and do not exist when the nonlocal corrections are incorporated (Fan and Zeigler 1992). In general, DFT predicts barrier heights that are lower than experiment, whereas *ab initio* calculations typically overestimate the measured values (Porezag and Pederson 1995; Deng, Branchadell, and Zeigler 1994). The inconsistencies in performance of DFT for different chemical systems indicate the need for metrics such as those presented here to gauge the usefulness and suitability of DFT methods.

In this paper, we report NDFT calculations for two possible decomposition mechanisms of *sym*-triazine ($H_3C_3N_3$):

sym-triazine ------> $(HCN)_3$ -------> 3HCN   (I)

sym-triazine ------> $HCN + H_2 C_2 N_2$ -----> 3HCN   (II)
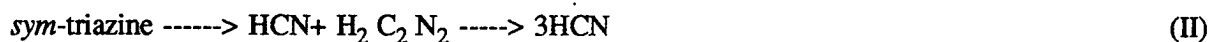
where $(HCN)_3$ denotes a hydrogen-bonded cyclic cluster of HCN molecules, and $H_2C_2N_2$ is a covalently bonded dimer. These reactions have been characterized in a previous *ab initio* study (Pai, Chabalowski,

and Rice 1996). In that work, critical points along the reaction coordinates for (I) and (II) were located through MP2 geometry optimizations using the 6-31G** (Hehre, Ditchfield, and Pople 1972; Hariharan and Pople 1973; Gordon 1980), 6-311++G** (McLean and Chandler 1980; Krishnan et al. 1980), and cc-pVTZ (Woon and Dunning 1993; Kendall, Dunning, and Harrison 1992; Dunning 1989) basis sets and characterized through normal mode analyses. Energy refinements of the MP2 structures were then performed at the QCISD(T) level. The results indicated that the low-energy path to decomposition of *sym*-triazine is through the concerted triple dissociation [Reaction (I)], in agreement with photodissociation experiments (Ondrey and Bersohn 1984). Also, the best prediction of the decomposition barrier (81.1 kcal/mol) is well below the experimentally measured upper limit (115 kcal/mol) (Ondrey and Bersohn 1984). Predictions of the reaction endothermicity of *sym*-triazine decomposition, however, were ~8 kcal/mol less than the experimental value (Ondrey and Bersohn 1984).

The NDFT results will be compared to the previously reported *ab initio* predictions (Pai, Chabalowski, and Rice, in press) and experiment, where available. In comparing quantum mechanical methods against each other and against experiment, we will use the results calculated with the cc-pVTZ basis set. Geometries, harmonic vibrational frequencies, and corresponding eigenvectors and relative energies of the critical points will be compared. Additionally, we will show the basis set size dependence of these methods.

For some properties, we are restricted to comparing the DFT results with the MP2 results due to either a lack of experimental data or results from a higher-level correlation technique. In these comparisons, it must be kept in mind that the MP2 results might or might not be more accurate than the DFT results. MP2 is a widely used method, and its strengths and weaknesses have been well-documented for many chemical properties. Therefore, MP2 serves as a useful metric. Even with our rather extensive computer resources, MP2 was the highest level of *ab initio* theory that we could perform on this size of system and still examine the basis set dependence.

2. METHODS

DFT calculations of critical points on the PES for *sym*-triazine reactions were performed using the GAUSSIAN 94 program package (Frisch et al. 1995). Geometry optimizations of stable and transition state species were done using the 6-31G** (Hehre, Ditchfield, and Pople 1972; Hariharan and Pople 1973; Gordon 1980), 6-311++G** (McLean and Chandler 1980; Krishnan et al. 1980), and cc-pVTZ (Woon and

Dunning 1993; Kendall, Dunning, and Harrison 1992; Dunning 1989) basis sets. The density functionals used are the various nonlocal spin density corrections to the local spin density (LSD) functional with the LSD exchange and the Vosko, Wilk, and Nusair (VWN) correlation functional (Vosko, Wilk, and Nusair 1980). These corrections were estimated by the exchange functional of Becke (1988) and the correlation energy function of Lee, Yang, and Parr (1988; Miehlich et al. 1989) (BLYP); the exchange functional of Becke and the correlation functional of Perdew (1986) (BP86); the exchange functional of Becke and the correlation functional of Perdew and Wang (1992) (BPW91); and the exchange functional described by the fitted three-parameter hybrid of Becke (1993) and the correlation functional of Lee, Yang, and Parr (B3LYP). All geometry optimizations met the default convergence criteria given by Gaussian 94 (Frisch et al. 1995). All critical points were characterized through normal mode analyses. IRC calculations for Reaction (I) using all functionals and the 6-31G** basis set were performed. The IRC calculations were terminated when minima were reached as defined by the default convergence criteria of the Gaussian 94 set of programs (Frisch 1995). All DFT calculations were performed using the default grid size given in Gaussian 94 (Frisch 1995).

3. RESULTS AND DISCUSSION

3.1 Geometries. The geometric parameters predicted at all levels for *sym*-triazine, the transition state, the weakly bound $(HCN)_3$ cluster, the dimer $(H_2C_2N_2)$, and the HCN molecule are listed in Table 1. *Ab initio* predictions from Pai, Chabalowski, and Rice (1996) are provided for comparison. Figure 1 shows structures corresponding to these critical points; the atom types and indices listed in Table 1 are denoted for *sym*-triazine, $(HCN)_3$, HCN, and $H_2C_2N_2$ in Figure 1. The internal coordinates used in our discussion are shown in the transition state structure in Figure 1(b) or the $(HCN)_3$ cluster [Figure 1(e)]. Although the atoms are not labeled on the transition state structure in Figure 1(b), the labeling of the atoms follows the same pattern around the ring as in Figure 1(a). The internal coordinates shown in Figure 1(b) will be discussed later and are the same for all structures illustrated in Figure 1.

3.1.1 Basis Set Dependence. The absolute percent differences of geometric parameters calculated using the 6-31G** or 6-311++G** basis sets relative to those calculated using the cc-pVTZ basis set are given in parentheses within the columns in Table 1 labeled "6-31G**" and "6-311++G**". The geometric parameters predicted by all methods for all critical points are insensitive to increasing basis set size ($\leq 1\%$), with two small exceptions. Firstly, the BLYP/6-31G** predictions of the elongated CN bonds in the

4

Table 1. Geometric Parameters for Critical Points on the *sym*-Triazine Potential Energy Surface

Parameter	MP2 [a] 6-31G**	MP2 6-311++G**	MP2 cc-pVTZ	BP86 6-31G**	BP86 6-311++G**	BP86 cc-pVTZ	BLYP 6-31G**	BLYP 6-311++G**	BLYP cc-pVTZ	B3LYP 6-31G**	B3LYP 6-311++G**	B3LYP cc-pVTZ	BPW91 6-31G**	BPW91 6-311++G**	BPW91 cc-pVTZ	Expt. [b,c,d]
sym-triazine																
C1N2	1.3404 (0)	1.3396 (0)	1.3351	1.3477 (0)	1.3445 (0)	1.3417	1.3505 (0)	1.3476 (0)	1.3443	1.3370 (0)	1.3342 (0)	1.3313	1.3463 (0)	1.3430 (0)	1.3403	1.338
C3N2	1.3404 (0)	1.3396 (0)	1.3351	1.3476 (0)	1.3443 (0)	1.3418	1.3505 (0)	1.3476 (0)	1.3443	1.3370 (0)	1.3341 (0)	1.3313	1.3463 (0)	1.3430 (0)	1.3403	1.338
C3N4	1.3404 (0)	1.3396 (0)	1.3351	1.3477 (0)	1.3444 (0)	1.3417	1.3506 (0)	1.3475 (0)	1.3443	1.3370 (0)	1.3342 (0)	1.3313	1.3463 (0)	1.3430 (0)	1.3403	1.338
C5N4	1.3404 (0)	1.3396 (0)	1.3351	1.3478 (0)	1.3446 (0)	1.3417	1.3506 (0)	1.3475 (0)	1.3443	1.3371 (0)	1.3343 (0)	1.3312	1.3463 (0)	1.3429 (0)	1.3403	1.338
C5N6	1.3404 (0)	1.3396 (0)	1.3351	1.3480 (0)	1.3448 (0)	1.3418	1.3507 (0)	1.3475 (0)	1.3442	1.3371 (0)	1.3344 (0)	1.3313	1.3463 (0)	1.3430 (0)	1.3403	1.338
C5H7	1.0833 (0)	1.0869 (0)	1.0822	1.0980 (0)	1.0959 (0)	1.0940	1.0959 (0)	1.0929 (0)	1.0908	1.0885 (0)	1.0862 (0)	1.0842	1.0959 (0)	1.0940 (0)	1.0924	1.084
C3H8	1.0833 (0)	1.0869 (0)	1.0822	1.0980 (0)	1.0959 (0)	1.0940	1.0959 (0)	1.0929 (0)	1.0908	1.0885 (0)	1.0862 (0)	1.0842	1.0959 (0)	1.0940 (0)	1.0924	1.084
C1H9	1.0833 (0)	1.0869 (0)	1.0822	1.0979 (0)	1.0958 (0)	1.0940	1.0959 (0)	1.0929 (0)	1.0908	1.0884 (0)	1.0862 (0)	1.0842	1.0959 (0)	1.0940 (0)	1.0924	1.084
C3N2C1	113.96 (0)	114.11 (0)	114.05	113.53 (0)	113.90 (0)	113.78	113.63 (0)	114.04 (0)	113.99	113.48 (0)	114.34 (0)	114.26	113.48 (0)	113.82 (0)	113.77	113.2
N4C3N2	126.04 (0)	125.89 (0)	125.95	126.52 (0)	126.16 (0)	126.21	126.40 (0)	125.95 (0)	126.01	126.03 (0)	125.70 (0)	125.73	126.51 (0)	126.17 (0)	126.23	126.8
C5N4C3	113.96 (0)	114.11 (0)	114.05	113.45 (0)	113.82 (0)	113.79	113.58 (0)	114.05 (0)	113.99	114.00 (0)	114.29 (0)	114.27	113.49 (0)	113.83 (0)	113.77	113.2
N6C5N4	126.04 (0)	125.89 (0)	125.95	126.54 (0)	126.18 (0)	126.21	126.41 (0)	125.96 (0)	126.01	126.04 (0)	125.71 (0)	125.73	126.51 (0)	126.17 (0)	126.23	126.8
N4C5H7	116.98 (0)	117.06 (0)	117.02	116.74 (0)	116.92 (0)	116.90	116.80 (0)	117.02 (0)	116.99	116.99 (0)	117.15 (0)	117.14	116.74 (0)	116.91 (0)	116.89	116.6
N2C3H8	116.98 (0)	117.06 (0)	117.02	116.73 (0)	116.92 (0)	116.89	116.80 (0)	117.02 (0)	116.99	116.99 (0)	117.15 (0)	117.13	116.74 (0)	116.91 (0)	116.89	116.6
N6C1H9	116.98 (0)	117.06 (0)	117.02	116.76 (0)	116.95 (0)	116.90	116.81 (0)	117.02 (0)	116.99	117.00 (0)	117.17 (0)	117.13	116.74 (0)	116.91 (0)	116.89	116.6
Transition state																
C1N2	1.2081 (1)	1.2039 (1)	1.1978	1.1974 (1)	1.1927 (0)	1.1889	1.2008 (1)	1.1964 (0)	1.1925	1.1883 (1)	1.1836 (0)	1.1800	1.1964 (1)	1.1915 (0)	1.1877	
C3N2	1.9024 (0)	1.8941 (0)	1.8980	2.0242 (0)	1.9936 (0)	1.9978	1.9995 (2)	1.9673 (0)	1.9680	1.9701 (1)	1.9444 (0)	1.9469	2.0232 (1)	1.9945 (0)	1.9963	
C3N4	1.2081 (1)	1.2039 (1)	1.1978	1.1975 (1)	1.1928 (0)	1.1889	1.2009 (1)	1.1964 (0)	1.1925	1.1884 (1)	1.1837 (0)	1.1800	1.1963 (1)	1.1915 (0)	1.1877	
C5N4	1.9024 (0)	1.8941 (0)	1.8980	2.0273 (0)	1.9971 (0)	1.9980	2.0012 (2)	1.9675 (0)	1.9681	1.9719 (1)	1.9464 (0)	1.9468	2.0231 (1)	1.9945 (0)	1.9964	
C5H7	1.0719 (0)	1.0756 (0)	1.0704	1.0813 (0)	1.0803 (0)	1.0780	1.0803 (1)	1.0786 (0)	1.0762	1.0733 (1)	1.0721 (1)	1.0697	1.0794 (1)	1.0784 (0)	1.0764	
C3H8	1.0719 (0)	1.0756 (0)	1.0704	1.0814 (0)	1.0804 (0)	1.0780	1.0804 (0)	1.0786 (0)	1.0762	1.0734 (0)	1.0721 (0)	1.0697	1.0794 (0)	1.0784 (0)	1.0764	
C1H9	1.0719 (0)	1.0756 (0)	1.0704	1.0813 (0)	1.0803 (0)	1.0780	1.0803 (0)	1.0787 (0)	1.0762	1.0733 (0)	1.0720 (0)	1.0697	1.0794 (0)	1.0784 (0)	1.0764	
C3N2C1	116.00 (0)	116.54 (0)	116.36	118.92 (0)	119.29 (0)	118.97	118.29 (0)	118.64 (0)	118.40	118.75 (0)	119.20 (0)	118.89	118.87 (0)	119.21 (0)	118.99	
N4C3N2	124.00 (0)	123.46 (0)	123.64	121.17 (0)	120.83 (0)	121.02	121.77 (0)	121.35 (0)	121.60	121.31 (0)	120.87 (0)	121.12	121.11 (0)	120.77 (0)	121.02	
C5N4C3	116.00 (0)	116.53 (0)	116.36	118.78 (0)	119.11 (0)	118.97	118.20 (0)	118.63 (0)	118.40	118.66 (0)	119.10 (0)	118.89	118.88 (0)	119.21 (0)	119.00	
N6C5N4	124.00 (0)	123.46 (0)	123.64	121.16 (0)	120.81 (0)	121.02	121.77 (0)	121.34 (0)	121.60	121.31 (0)	120.86 (0)	121.12	121.11 (0)	120.76 (0)	121.01	
N4C5H7	97.00 (1)	97.03 (1)	96.27	92.69 (1)	93.79 (0)	93.41	94.26 (1)	95.46 (0)	95.18	93.78 (1)	94.71 (0)	94.41	92.87 (1)	93.87 (0)	93.45	
N2C3H8	97.00 (0)	97.03 (0)	96.27	92.79 (1)	93.88 (1)	93.41	94.31 (1)	95.46 (0)	95.18	93.84 (1)	94.76 (0)	94.41	92.87 (1)	93.87 (0)	93.45	
N6C1H9	97.00 (1)	97.04 (1)	96.27	92.78 (1)	93.89 (1)	93.42	94.32 (1)	95.49 (0)	95.18	93.84 (1)	94.77 (0)	94.41	92.89 (1)	93.90 (1)	93.43	
HCN																
CN	1.1778 (1)	1.1714 (0)	1.1668	1.1696 (1)	1.1615 (0)	1.1586	1.1691 (1)	1.1606 (0)	1.1575	1.1572 (1)	1.1491 (0)	1.1463	1.1685 (1)	1.1604 (0)	1.1577	1.1570
CH	1.0649 (0)	1.0680 (0)	1.0643	1.0778 (0)	1.0758 (0)	1.0745	1.0757 (0)	1.0729 (0)	1.0712	1.0691 (0)	1.0668 (0)	1.0653	1.0760 (0)	1.0739 (0)	1.0729	1.0580
HCN	180.00 (0)	180.00 (0)	180.00	180.00 (0)	180.00 (0)	180.00	180.00 (0)	180.00 (0)	180.00	180.00 (0)	180.00 (0)	180.00	180.00 (0)	180.00 (0)	180.00	180.00

5

[a] Pai, Chabalowski, and Rice (1996).

[b] Lancaster and Stoicheff (1956).

[c] Herzberg (1945).

[d] Huber and Herzberg (1979).

Table 1. Geometric Parameters for Critical Points on the *sym*-Triazine Potential Energy Surface (continued)

Parameter	MP2[a]			BP86			BLYP			B3LYP			BPW91			Expt.[b,c,d]
	6-31G**	6-311++G**	cc-pVTZ	6-31G**	6-311++G**	cc-pVTZ	6-31G**	6-311++G**	cc-pVTZ	6-31G**	6-311++G**	cc-pVTZ	6-31G**	6-311++G**	cc-pVTZ	
(HCN)₃																
C1N2	1.1773 (1)	1.1710 (0)	1.1665	1.1697 (1)	1.1615 (0)	1.1586	1.1692 (1)	1.1605 (0)	1.1574	1.1574 (1)	1.1492 (0)	1.1463	1.1684 (1)	1.1603 (0)	1.1575	
C3N2	3.1537 (1)	3.1682 (1)	3.1290	3.1551 (1)	3.1976 (0)	3.1990	3.2019 (2)	3.2689 (0)	3.2597	3.1672 (2)	3.2097 (0)	3.2064	3.2374 (2)	3.3052 (0)	3.3161	
C3N4	1.1774 (1)	1.1710 (0)	1.1665	1.1697 (1)	1.1615 (0)	1.1586	1.1692 (1)	1.1605 (0)	1.1574	1.1574 (1)	1.1492 (0)	1.1463	1.1685 (1)	1.1603 (0)	1.1575	
C5N4	3.1539 (1)	3.1682 (1)	3.1291	3.1612 (1)	3.2075 (0)	3.2088	3.2062 (2)	3.2777 (0)	3.2581	3.1701 (1)	3.2149 (0)	3.2071	3.2448 (2)	3.3178 (0)	3.3134	
C5N6	1.1773 (1)	1.1710 (0)	1.1665	1.1697 (1)	1.1615 (0)	1.1586	1.1692 (1)	1.1605 (0)	1.1574	1.1574 (1)	1.1492 (0)	1.1463	1.1684 (1)	1.1602 (0)	1.1575	
C5H7	1.0680 (0)	1.0707 (0)	1.0678	1.0829 (0)	1.0796 (0)	1.0787	1.0796 (0)	1.0759 (0)	1.0746	1.0732 (0)	1.0701 (0)	1.0689	1.0798 (0)	1.0768 (0)	1.0760	
C3H8	1.0680 (0)	1.0708 (0)	1.0679	1.0832 (0)	1.0799 (0)	1.0789	1.0798 (0)	1.0761 (0)	1.0746	1.0734 (0)	1.0703 (0)	1.0689	1.0801 (0)	1.0771 (0)	1.0761	
C1H9	1.0680 (0)	1.0707 (0)	1.0678	1.0830 (0)	1.0797 (0)	1.0787	1.0796 (0)	1.0760 (0)	1.0745	1.0732 (0)	1.0702 (0)	1.0688	1.0799 (0)	1.0769 (0)	1.0760	
N6C5H7	182.99 (0)	182.32 (0)	182.93	183.66 (0)	182.89 (0)	183.07	183.47 (0)	182.75 (0)	182.81	183.27 (0)	182.65 (0)	182.82	183.12 (0)	182.41 (0)	182.54	
N2H8C3	122.13 (1)	119.45 (2)	121.48	128.28 (3)	124.38 (0)	124.51	127.60 (4)	123.29 (0)	123.03	126.22 (3)	122.35 (0)	122.64	127.58 (3)	123.65 (0)	123.53	
H8N2C1	120.92 (1)	122.92 (1)	121.56	116.37 (2)	119.79 (0)	119.21	116.82 (3)	120.54 (0)	119.98	117.79 (2)	121.15 (1)	120.40	116.68 (2)	119.88 (1)	119.21	
N2H8	2.4532 (1)	2.5014 (3)	2.4359	2.3673 (4)	2.4610 (0)	2.4618	2.4266 (5)	2.5521 (0)	2.5471	2.4123 (4)	2.5070 (0)	2.5010	2.4634 (5)	2.5844 (5)	2.5981	
dimer																
C1N2	1.2893 (0)	1.2871 (0)	1.2837	1.2957 (1)	1.2909 (0)	1.2880	1.2962 (1)	1.2911 (0)	1.2878	1.2831 (1)	1.2788 (0)	1.2761	1.2944 (1)	1.2892 (0)	1.2869	
C3N2	1.5369 (0)	1.5369 (0)	1.5339	1.5440 (0)	1.5415 (0)	1.5412	1.5541 (0)	1.5517 (0)	1.5512	1.5295 (0)	1.5263 (0)	1.5254	1.5409 (0)	1.5387 (0)	1.5387	
C3N4	1.2895 (0)	1.2871 (0)	1.2837	1.2957 (1)	1.2909 (0)	1.2880	1.2962 (1)	1.2911 (0)	1.2878	1.2831 (1)	1.2788 (0)	1.2761	1.2944 (1)	1.2892 (0)	1.2869	
C3H8	1.0845 (0)	1.0893 (0)	1.0846	1.1009 (0)	1.0990 (0)	1.0967	1.0988 (0)	1.0959 (0)	1.0941	1.0909 (0)	1.0887 (0)	1.0868	1.0988 (0)	1.0964 (0)	1.0951	
C1H9	1.0845 (0)	1.0893 (0)	1.0846	1.1009 (0)	1.0990 (0)	1.0967	1.0988 (0)	1.0959 (0)	1.0941	1.0909 (0)	1.0887 (0)	1.0868	1.0988 (0)	1.0964 (0)	1.0951	
C3N2C1	79.35 (0)	79.71 (0)	79.56	79.15 (0)	79.63 (0)	79.51	79.54 (0)	80.07 (0)	79.91	79.79 (0)	80.29 (0)	80.11	79.09 (0)	79.56 (0)	79.43	
N4C3N2	100.61 (0)	100.29 (0)	100.44	100.85 (0)	100.37 (0)	100.49	100.46 (0)	99.93 (0)	100.09	100.21 (0)	99.71 (0)	99.89	100.91 (0)	100.44 (0)	100.57	
N2C3H8	131.91 (0)	132.30 (0)	131.84	131.04 (0)	131.29 (0)	131.27	131.27 (0)	131.58 (0)	131.46	131.30 (0)	131.55 (0)	131.41	131.03 (0)	131.36 (0)	131.24	
N2C1H9	131.88 (0)	132.30 (0)	131.84	131.04 (0)	131.29 (0)	131.27	131.27 (0)	131.58 (0)	131.46	131.30 (0)	131.55 (0)	131.41	131.03 (0)	131.36 (0)	131.24	

6

[a] Pai, Chabalowski, and Rice (1996).
[b] Lancaster and Stoicheff (1956).
[c] Herzberg (1945).
[d] Huber and Herzberg (1979).
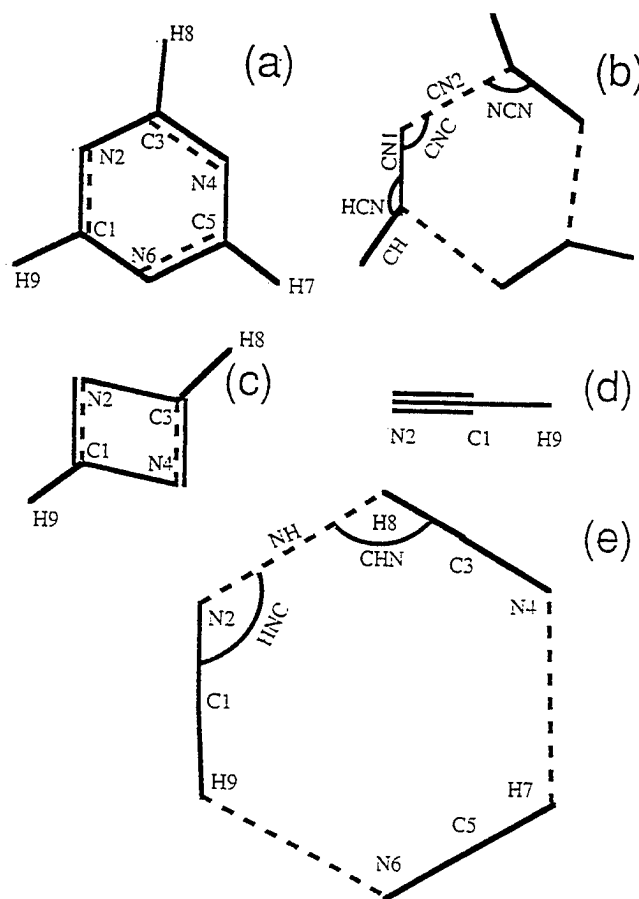
Figure 1. Structures of (a) *sym*-triazine, (b) the transition state for the concerted triple dissociation reaction [Reaction (I)], (c) the dimer species $H_2C_2N_2$ associated with the stepwise decomposition reaction [Reaction (II)], (d) the HCN molecule, and (e) the $(HCN)_3$ cluster located on the concerted triple dissociation reaction path.

transition state are 2% larger than the predictions using the cc-pVTZ basis set. Increasing the basis set to 6-311++G** brings the BLYP predictions of this bond length to within a percent of the cc-pVTZ value.

Secondly, all DFT predictions of intermolecular geometric parameters (N-H distances and CNH and NHC angles) in the weakly bound $(HCN)_3$ cluster show a small basis set dependence (1–5%). All DFT/6-31G** predictions of the N-H bond distance differ by at least 4% from the DFT/cc-pVTZ predictions, but increasing the basis set size to 6-311++G** reduces the difference to within 1% for all DFT calculations. Similarly, the DFT/6-31G** intermolecular bond angles differ by 2–4% from the cc-pVTZ values, but are improved upon increasing the basis set to 6-311++G**. It is interesting to note that for the MP2 results, increasing the basis set size from 6-31G** to 6-311++G** increased the percent difference with the cc-pVTZ results in these intermolecular geometric parameters.

7

3.1.2 Method Comparison. Figure 2 provides a comparison of DFT structural parameters using the cc-pVTZ basis set with experiment where available or with MP2 geometries when experiment is unavailable. For those species for which experimental data exist, the ordinate axis label is entitled "% Error". For those species for which experimental data do not exist, the ordinate axis label is titled "% Deviation" and refers to the deviation from the MP2/cc-pVTZ predictions. In addition, for those structures for which experimental data exist, MP2 predictions are provided for additional comparison. A positive or negative percent deviation from the standard (experiment or MP2) represents an overestimation or underestimation, respectively, of that structural parameter. The labels along the abscissa denote the internal coordinates of the species according to the labeling of structures in Figures 1(b) and 1(e).
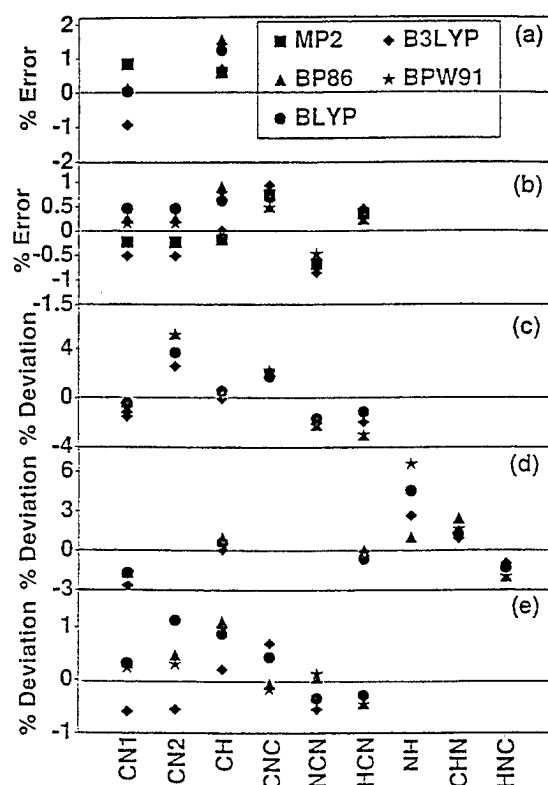
Figure 2. Percent error from experiment for the structural parameters of (a) HCN and (b) sym-triazine for all methods using the cc-pVTZ basis set. Percent deviation of DFT/cc-pVTZ methods from MP2/cc-pVTZ for (c) the transition state, (d) the $(HCN)_3$ cluster, and (e) $H_2C_2N_2$. Method is denoted by symbols in the legend in Figure 2(a). See Figure 1(b) and (e) for definition of internal coordinates shown along the abscissa.

Geometric parameters of HCN and sym-triazine [Figures 2(a) and 2(b), respectively,] predicted by all methods are within 2% of experiment. DFT predictions of structural parameters for the transition state [Figure 2(c)] are within 4% of the MP2 predictions, except for the CN2 bond, which is being broken as

8

the *sym*-triazine proceeds along the reaction path. For that parameter, the B3LYP prediction is in closest agreement to the MP2 prediction. The BPW91 and BP86 values overestimate the MP2 value by ~5% (~0.1 Å). Similarly, all of the DFT predictions of structural parameters of the $(HCN)_3$ cluster [Figure 2(d)] are within 3% of the MP2 values, except for the weak N-H hydrogen bond. The BP86 prediction of this bond distance is in closest agreement with the MP2 (1%), followed by the B3LYP prediction (~3%). The BPW91 prediction of the N-H bond exceeds the MP2 prediction by ~6% (0.16 Å). DFT predictions of the structure of the dimer species agree with MP2 to within 1.5%.

The good agreement of DFT with experiment suggests that the DFT predictions of structural parameters for stable, covalently bonded structures on the *sym*-triazine PES are as good as MP2. Also, the small basis set dependence of the DFT geometries indicates that reasonably accurate structural parameters can be obtained using a small basis set (6-31G**). The agreement of DFT with MP2 is better for HCN, *sym*-triazine, and the dimer than for the transition state and loosely bound cluster. However, the DFT predictions differ from MP2 by no more than 7%.

3.2 Vibrational Analyses. Normal mode analyses of all critical points on the *sym*-triazine PES using DFT methods and the 6-31G**, 6-311++G**, and cc-pVTZ basis sets were performed, and the harmonic vibrational frequencies at all levels are reported in Table 2. MP2 eigenvectors corresponding to the frequencies listed in Table 2 for *sym*-triazine, the transition state, the $(HCN)_3$ cluster, and the $H_2C_2N_2$ dimer are shown in Figures 3–6, respectively.

The assignment of the MP2 modes for *sym*-triazine to experiment is discussed extensively in Pai, Chabalowski, and Rice (1996). The assignments to experiment are based upon visual inspection of the MP2 eigenvectors of *sym*-triazine (Figure 3) and the description of the atomic motions given in the experimental paper by Lancaster, Stamm, and Colthup (1961). DFT mode assignments are based upon comparison of the DFT eigenvectors with the MP2 eigenvectors rather than simply matching the harmonic frequencies. The comparison is accomplished by projecting the DFT eigenvectors onto all choices of MP2 eigenvectors subject to similarity apparent from visual inspection and within a reasonable energy range.

Assigning some of the low-frequency (<150 cm^{-1}) DFT-vibrational modes of the $(HCN)_3$ cluster to the MP2 modes was difficult. For example, Figure 7 shows three pairs of MP2/cc-pVTZ and BPW91/ cc-pVTZ eigenvectors that we were unable to match through visual inspection. The MP2/cc-pVTZ

Table 2. Harmonic Vibrational Frequencies (cm^{-1})

Mode	MP2[a] 6-31G**	MP2 6-311++G**	MP2 cc-pVTZ	BP86 6-31G**	BP86 6-311++G**	BP86 cc-pVTZ	BLYP 6-31G**	BLYP 6-311++G**	BLYP cc-pVTZ	B3LYP 6-31G**	B3LYP 6-311++G**	B3LYP cc-pVTZ	BPW91 6-31G**	BPW91 6-311++G**	BPW91 cc-pVTZ	EXPT[b,c,d,e]
syn-triazine																
1	358 (0)	341 (-17)	358	313 (0)	310 (-3)	313	322 (-2)	320 (-4)	324	351 (-1)	348 (-4)	352	312 (0)	310 (-2)	312	340
2	358 (0)	341 (-17)	358	314 (0)	312 (-2)	314	323 (-2)	321 (-4)	325	352 (-1)	349 (-4)	353	313 (0)	312 (-1)	313	340
3	687 (4)	686 (3)	683	667 (0)	670 (3)	667	669 (-2)	672 (1)	671	692 (-1)	695 (2)	693	669 (1)	671 (3)	668	675
4	687 (4)	686 (3)	683	667 (0)	670 (3)	667	670 (-1)	672 (1)	671	692 (-1)	695 (2)	693	669 (1)	672 (4)	668	675
5	770 (-2)	744 (-28)	772	739 (-1)	732 (-8)	740	740 (-1)	733 (-8)	741	759 (-2)	752 (-9)	761	740 (-2)	734 (-8)	742	737
6	921 (-19)	895 (-45)	940	899 (-9)	898 (-10)	908	898 (-12)	900 (-10)	910	944 (-12)	944 (-12)	956	903 (-9)	904 (-8)	912	925
7	1015 (5)	1014 (4)	1010	973 (-2)	975 (-9)	971	967 (3)	966 (2)	964	1015 (4)	1015 (4)	1011	976 (4)	978 (4)	974	992
8	1027 (-16)	957 (-86)	1043	994 (-9)	979 (-24)	1003	993 (-11)	982 (-22)	1004	1037 (-12)	1024 (-25)	1049	998 (-9)	986 (-21)	1007	1031
9	1027 (-17)	957 (-87)	1044	995 (-9)	980 (-24)	1004	994 (-11)	983 (-22)	1005	1038 (-12)	1025 (-25)	1050	998 (-9)	986 (-21)	1007	1031
10	1145 (1)	1140 (-4)	1144	1120 (-4)	1118 (-6)	1124	1146 (22)	1118 (-6)	1124	1157 (-4)	1154 (-7)	1161	1123 (-3)	1121 (-5)	1126	1132
11	1212 (13)	1200 (1)	1199	1162 (5)	1160 (3)	1157	1152 (5)	1146 (-1)	1147	1204 (7)	1197 (0)	1197	1166 (4)	1164 (2)	1162	1174
12	1212 (13)	1200 (1)	1199	1163 (7)	1158 (2)	1156	1153 (6)	1145 (-2)	1147	1204 (7)	1197 (0)	1197	1167 (6)	1163 (2)	1161	1174
13	1256 (13)	1232 (-11)	1243	1182 (28)	1157 (-1)	1154	1120 (1)	1116 (1)	1115	1198 (31)	1170 (3)	1167	1184 (26)	1162 (4)	1158	1251
14	1469 (20)	1452 (3)	1449	1396 (6)	1389 (-1)	1390	1395 (6)	1386 (-3)	1389	1449 (6)	1440 (-3)	1443	1403 (7)	1395 (-1)	1396	1410
15	1469 (20)	1452 (3)	1449	1398 (8)	1390 (0)	1390	1395 (6)	1386 (-3)	1389	1450 (7)	1441 (-2)	1443	1403 (7)	1396 (0)	1396	1410
16	1622 (22)	1600 (0)	1600	1541 (14)	1529 (2)	1527	1524 (15)	1507 (2)	1509	1611 (17)	1595 (1)	1594	1547 (13)	1536 (2)	1534	1556
17	1622 (22)	1600 (0)	1600	1542 (15)	1529 (2)	1527	1525 (16)	1508 (-1)	1509	1611 (17)	1595 (1)	1594	1547 (13)	1536 (2)	1534	1556
18	1430 (25)	1411 (6)	1405	1361 (7)	1351 (-3)	1354	1371 (6)	1360 (-5)	1365	1409 (5)	1399 (-5)	1404	1368 (8)	1358 (-2)	1360	1617
19	3272 (47)	3225 (0)	3225	3100 (22)	3090 (12)	3078	3098 (16)	3086 (4)	3082	3186 (21)	3173 (8)	3165	3111 (21)	3098 (8)	3090	3042
20	3268 (47)	3221 (0)	3221	3094 (21)	3084 (11)	3073	3092 (15)	3080 (3)	3077	3180 (20)	3168 (8)	3160	3105 (20)	3093 (8)	3085	3056
21	3268 (47)	3221 (0)	3221	3094 (21)	3085 (12)	3073	3092 (15)	3081 (4)	3077	3181 (21)	3168 (8)	3160	3106 (21)	3093 (8)	3085	3056
z.p.e	41.6	40.9	41.2	39.6	39.4	39.4	39.5	39.3	39.4	41.1	40.8	40.9	39.8	39.6	39.6	40.5
transition state																
1	725i (27)	725i (27)	698i	499i (-19)	522i (4)	518i	525i (-23)	550i (2)	547i	612i (-20)	636i (4)	632i	504i (18)	526i (4)	522i	
2	152 (12)	120 (-20)	140	124 (-4)	126 (2)	128	137 (-7)	146 (2)	144	142 (-5)	145 (3)	147	129 (1)	132 (4)	128	
3	152 (11)	120 (-21)	141	126 (-2)	129 (1)	128	138 (-6)	146 (2)	144	144 (-4)	148 (0)	148	129 (1)	133 (5)	128	
4	307 (-9)	309 (-7)	316	243 (-11)	248 (-6)	254	252 (-12)	259 (-5)	264	261 (-12)	265 (-8)	273	243 (-9)	248 (-4)	252	
5	307 (-9)	309 (-7)	316	245 (-9)	250 (-4)	254	253 (-12)	260 (-5)	265	262 (-11)	266 (-7)	273	243 (-9)	249 (-3)	252	
6	361 (8)	332 (-21)	353	283 (-9)	295 (3)	292	306 (-15)	323 (2)	321	317 (-9)	327 (1)	326	286 (-6)	297 (5)	292	
7	551 (0)	552 (1)	551	466 (-15)	477 (-4)	481	482 (-17)	497 (-2)	499	504 (-14)	514 (-4)	518	469 (-12)	480 (-1)	481	
8	551 (0)	552 (1)	551	467 (-15)	478 (-4)	482	483 (-17)	497 (-3)	500	505 (-14)	515 (-4)	519	469 (-12)	480 (-2)	482	
9	614 (17)	614 (17)	597	521 (-15)	540 (4)	536	546 (-20)	568 (2)	566	570 (-14)	587 (3)	584	524 (-13)	541 (4)	537	
10	784 (-2)	770 (-16)	786	738 (-9)	747 (0)	747	738 (-13)	750 (-1)	751	781 (-12)	791 (-2)	793	742 (-9)	752 (1)	751	
11	824 (-3)	789 (-38)	827	762 (-10)	770 (-2)	772	768 (-13)	779 (-2)	781	809 (-12)	818 (-3)	821	766 (-9)	775 (0)	775	
12	824 (-3)	789 (-38)	827	763 (-9)	771 (-2)	772	769 (-12)	779 (-2)	781	810 (-11)	818 (-3)	821	767 (-9)	776 (1)	776	
13	1011 (29)	1002 (20)	982	889 (-8)	903 (6)	897	914 (-12)	930 (4)	926	963 (-7)	975 (5)	970	895 (-7)	907 (5)	902	
14	1095 (37)	1079 (21)	1058	958 (-5)	968 (5)	963	991 (-9)	1003 (2)	1000	1038 (-4)	1046 (4)	1042	964 (-4)	974 (6)	968	
15	1095 (37)	1080 (22)	1058	959 (-5)	971 (7)	964	992 (-8)	1003 (3)	1000	1039 (-3)	1046 (4)	1042	965 (-4)	974 (5)	969	
16	1788 (8)	1756 (-24)	1780	1844 (23)	1810 (-11)	1821	1805 (27)	1768 (-10)	1778	1874 (27)	1838 (-9)	1847	1852 (25)	1819 (-8)	1827	
17	1943 (12)	1915 (-16)	1931	1967 (14)	1943 (-10)	1953	1942 (16)	1916 (-10)	1926	2032 (18)	2005 (-9)	2014	1975 (16)	1953 (-6)	1959	
18	1943 (12)	1915 (-16)	1931	1968 (15)	1944 (-9)	1953	1942 (15)	1916 (-10)	1926	2033 (19)	2005 (-9)	2014	1976 (16)	1953 (-7)	1960	
19	3415 (50)	3357 (-8)	3365	3302 (29)	3273 (0)	3273	3286 (29)	3254 (-3)	3257	3375 (31)	3342 (-2)	3344	3319 (33)	3286 (0)	3286	
20	3415 (50)	3357 (-8)	3365	3304 (31)	3274 (1)	3273	3288 (31)	3255 (-2)	3257	3376 (32)	3343 (-1)	3344	3319 (32)	3287 (0)	3287	
21	3418 (51)	3359 (-8)	3367	3304 (30)	3275 (1)	3274	3288 (30)	3255 (-3)	3258	3376 (31)	3344 (-1)	3345	3319 (32)	3287 (0)	3287	
z.p.e	35.1	34.4	34.7	33.2	33.2	33.2	33.3	33.3	33.4	34.6	34.5	34.6	33.4	33.3	33.3	

[a] Pai, Chabalowski, and Rice (1996).
[b] Herzberg (1945).
[c] Huber and Herzberg (1979).
[d] Lancaster, Stamm, and Colhup (1961).
[e] Jucks and Miller (1988).

10

Table 2. Harmonic Vibrational Frequencies (cm⁻¹) (continued)

Mode	MP2[a] 6-31G**	MP2 6-311++G**	MP2 cc-pVTZ	BP86 6-31G**	BP86 6-311++G**	BP86 cc-pVTZ	BLYP 6-31G**	BLYP 6-311++G**	BLYP cc-pVTZ	B3LYP 6-31G**	B3LYP 6-311++G**	B3LYP cc-pVTZ	BPW91 6-31G**	BPW91 6-311++G**	BPW91 cc-pVTZ	Expt[b,c,d,e]
HCN																
1	725 (6)	730 (11)	719	732 (9)	728 (5)	723	734 (9)	728 (3)	725	769 (7)	766 (4)	762	736 (9)	732 (5)	727	712
2	725 (6)	730 (11)	719	732 (9)	728 (5)	723	734 (9)	728 (3)	725	769 (7)	766 (4)	762	736 (9)	732 (5)	727	712
3	2039 (12)	2016 (-11)	2027	2125 (10)	2111 (-4)	2115	2122 (9)	2106 (-7)	2113	2214 (13)	2196 (-5)	2201	2132 (10)	2118 (-4)	2122	2089
4	3533 (57)	3482 (6)	3476	3386 (23)	3368 (5)	3363	3388 (19)	3372 (3)	3369	3476 (25)	3454 (3)	3451	3402 (26)	3384 (8)	3376	3312
z.p.e	10.0	10.0	9.9	10.0	10.0	9.9	10.0	10.0	9.9	10.3	10.3	10.3	10.0	10.0	9.9	9.9
(HCN)3																
1	50 (-3)	46 (-7)	53	59 (6)	52 (-1)	53	59 (6)	51 (-2)	53	60 (5)	55 (0)	55	52 (6)	44 (-2)	46	
2	50 (-3)	46 (-7)	53	62 (6)	56 (0)	56	61 (4)	55 (-1)	56	61 (4)	57 (0)	57	56 (5)	51 (0)	51	
3	83 (1)	74 (-8)	82	92 (7)	86 (1)	85	89 (6)	83 (0)	83	91 (6)	86 (1)	85	88 (8)	81 (2)	79	
4	83 (1)	74 (-8)	82	94 (8)	87 (1)	86	90 (6)	84 (0)	84	92 (6)	87 (1)	86	86 (8)	80 (2)	78	
5	105 (-4)	102 (-7)	109	109 (12)	98 (1)	97	107 (15)	92 (-3)	95	112 (10)	101 (-1)	102	95 (17)	80 (1)	79	
6	136 (2)	121 (-13)	134	145 (9)	139 (3)	136	149 (17)	133 (1)	132	145 (8)	140 (3)	137	137 (11)	129 (3)	126	
7	148 (6)	133 (-9)	142	154 (20)	136 (2)	134	140 (9)	129 (2)	131	156 (17)	140 (1)	139	137 (15)	123 (1)	122	
8	155 (10)	140 (-5)	145	136 (23)	113 (0)	113	132 (21)	103 (-8)	111	144 (20)	120 (1)	124	109 (23)	84 (-2)	86	
9	155 (10)	140 (-5)	145	135 (26)	110 (-3)	109	134 (30)	99 (-5)	104	142 (23)	117 (-2)	119	106 (28)	78 (0)	78	
10	729 (0)	735 (6)	729	744 (9)	735 (0)	735	746 (9)	738 (1)	737	785 (7)	779 (1)	778	747 (6)	741 (0)	741	
11	730 (1)	735 (6)	729	745 (11)	736 (2)	734	748 (12)	739 (3)	736	785 (8)	780 (3)	777	748 (8)	742 (8)	740	
12	740 (7)	740 (7)	733	750 (12)	740 (3)	738	754 (13)	743 (2)	741	790 (10)	782 (3)	780	754 (9)	746 (1)	745	
13	778 (9)	771 (2)	769	792 (20)	773 (1)	772	789 (19)	770 (0)	770	826 (17)	810 (1)	809	789 (20)	771 (2)	769	327.1
14	786 (12)	778 (4)	774	794 (22)	775 (3)	772	790 (21)	772 (3)	769	827 (18)	811 (2)	809	790 (24)	773 (5)	768	
15				803 (25)	781 (3)	778	799 (24)	777 (2)	775	834 (21)	816 (3)	813	798 (21)	778 (4)	774	
16	2046 (13)	2023 (-10)	2033	2120 (7)	2108 (-5)	2113	2118 (5)	2106 (-7)	2113	2210 (11)	2194 (-5)	2199	2129 (8)	2117 (-4)	2121	
17	2046 (13)	2023 (-10)	2033	2121 (7)	2109 (-5)	2114	2118 (5)	2106 (-7)	2113	2210 (11)	2194 (-5)	2199	2129 (7)	2118 (-3)	2121	
18	2049 (14)	2025 (-10)	2035	2122 (7)	2110 (-5)	2115	2119 (5)	2107 (-7)	2114	2211 (10)	2195 (-6)	2201	2130 (7)	2119 (-1)	2123	
19	3496 (63)	3451 (18)	3433	3322 (11)	3320 (9)	3311	3339 (11)	3336 (6)	3330	3426 (17)	3415 (6)	3409	3354 (14)	3348 (8)	3340	
20	3501 (63)	3454 (16)	3438	3328 (12)	3325 (9)	3316	3345 (11)	3340 (6)	3334	3432 (18)	3419 (5)	3414	3359 (16)	3352 (9)	3343	3274
21	3501 (63)	3456 (18)	3438	3330 (12)	3327 (9)	3318	3346 (11)	3341 (6)	3335	3433 (19)	3420 (6)	3414	3361 (17)	3354 (10)	3344	
z.p.e	31.7	31.2	31.2	31.4	31.0	31.0	31.4	31.0	31.0	32.6	32.2	32.2	31.4	31.0	31.0	
dimer																
1	438 (10)	419 (-9)	428	390 (-1)	389 (-2)	391	413 (-3)	411 (-5)	416	427 (1)	423 (-3)	426	388 (-1)	385 (-4)	389	
2	737 (12)	734 (9)	725	679 (9)	678 (8)	670	641 (11)	639 (9)	630	717 (5)	719 (7)	712	688 (9)	687 (8)	679	
3	791 (-15)	790 (-16)	806	780 (-10)	789 (-1)	790	770 (-14)	780 (-4)	784	831 (-13)	838 (-6)	844	786 (-10)	793 (-3)	796	
4	882 (2)	881 (1)	880	876 (2)	878 (4)	874	877 (3)	877 (3)	874	927 (1)	930 (4)	926	876 (2)	878 (4)	874	
5	919 (-15)	886 (-48)	934	908 (-10)	901 (-17)	918	900 (0)	895 (-5)	900	946 (-10)	940 (-16)	956	914 (-10)	906 (-18)	924	
6	1015 (22)	1006 (13)	993	933 (13)	926 (6)	920	913 (0)	906 (-6)	912	968 (3)	963 (4)	959	939 (14)	932 (7)	925	
7	1241 (27)	1211 (-3)	1214	1171 (9)	1161 (-1)	1162	1170 (6)	1159 (-5)	1164	1214 (7)	1202 (-5)	1207	1177 (9)	1166 (-2)	1168	
8	1266 (27)	1239 (0)	1239	1199 (10)	1189 (0)	1189	1199 (8)	1188 (-3)	1191	1242 (8)	1231 (-3)	1234	1206 (11)	1195 (0)	1195	
9	1625 (29)	1597 (1)	1596	1560 (10)	1550 (0)	1550	1549 (10)	1537 (-2)	1539	1626 (16)	1611 (1)	1610	1566 (11)	1559 (0)	1556	
10	1697 (37)	1672 (12)	1660	1593 (13)	1580 (0)	1580	1577 (12)	1562 (-3)	1565	1664 (17)	1646 (-1)	1647	1600 (13)	1590 (3)	1587	
11	3258 (54)	3203 (-1)	3204	3063 (11)	3054 (2)	3052	3064 (14)	3056 (6)	3050	3160 (18)	3148 (6)	3142	3080 (16)	3074 (10)	3064	
12	3260 (54)	3205 (-1)	3206	3066 (11)	3058 (3)	3055	3067 (15)	3059 (7)	3052	3163 (18)	3151 (6)	3145	3082 (15)	3078 (11)	3067	
z.p.e	24.5	24.1	24.1	23.2	23.1	23.1	23.1	23.0	23.0	24.1	24.0	24.0	23.2	23.3	23.2	

[a] Pai, Chabalowski, and Rice (1996).
[b] Herzberg (1945).
[c] Huber and Herzberg (1979).
[d] Lancaster, Stamm, and Colthup (1961).
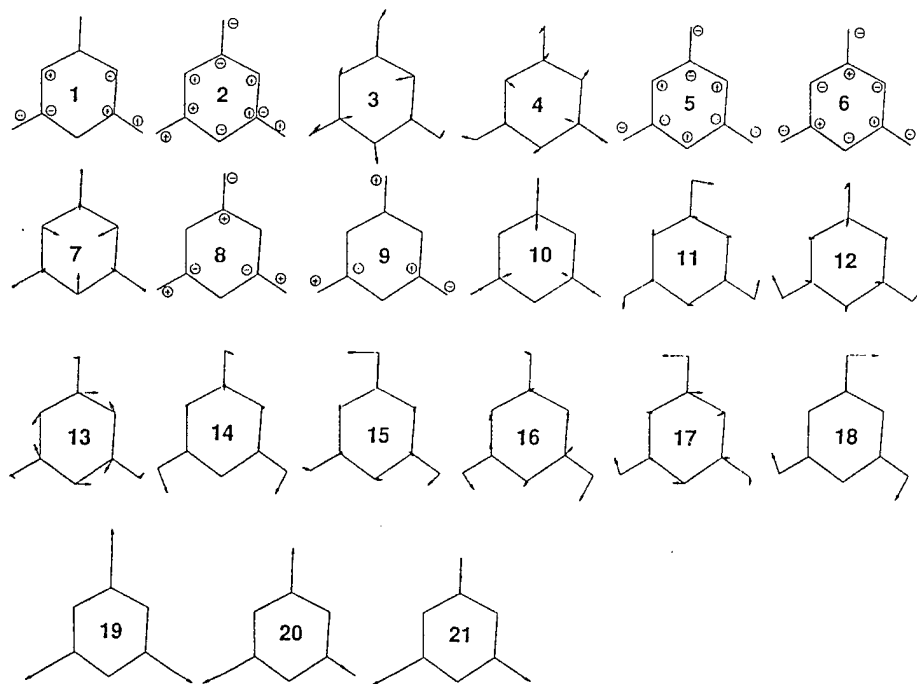[e] Jucks and Miller (1988).

Figure 3. MP2/cc-pVTZ eigenvectors corresponding to harmonic vibrational frequencies (given in Table 2) for *sym*-triazine. Positive and negative signs denote out-of-plane motion.
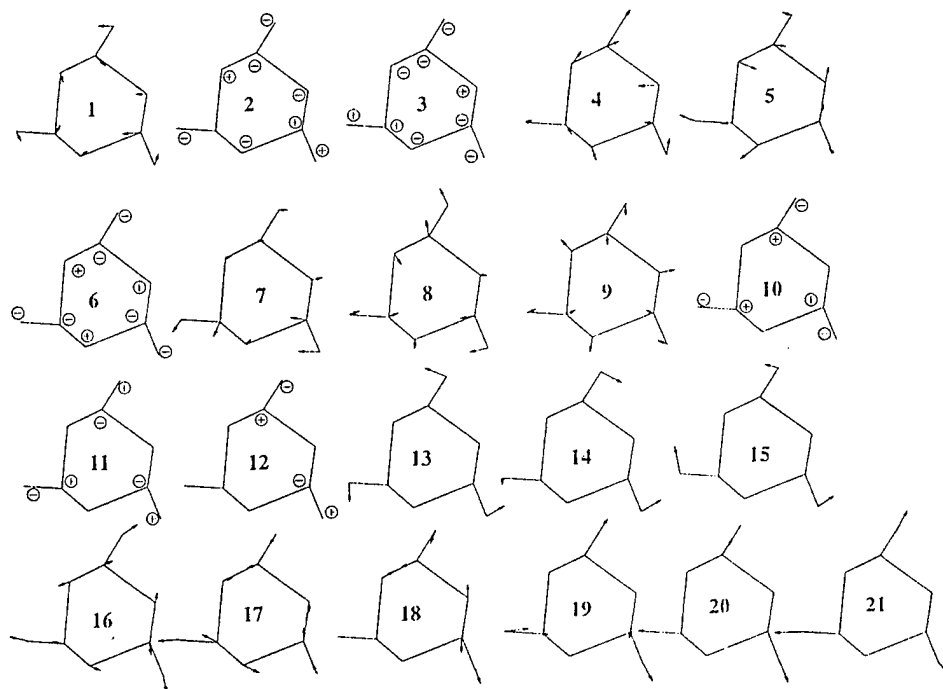

Figure 4. MP2/cc-pVTZ eigenvectors corresponding to harmonic vibrational frequencies (given in Table 2) for the transition state for Reaction (I). Positive and negative signs denote out-of-plane motion.
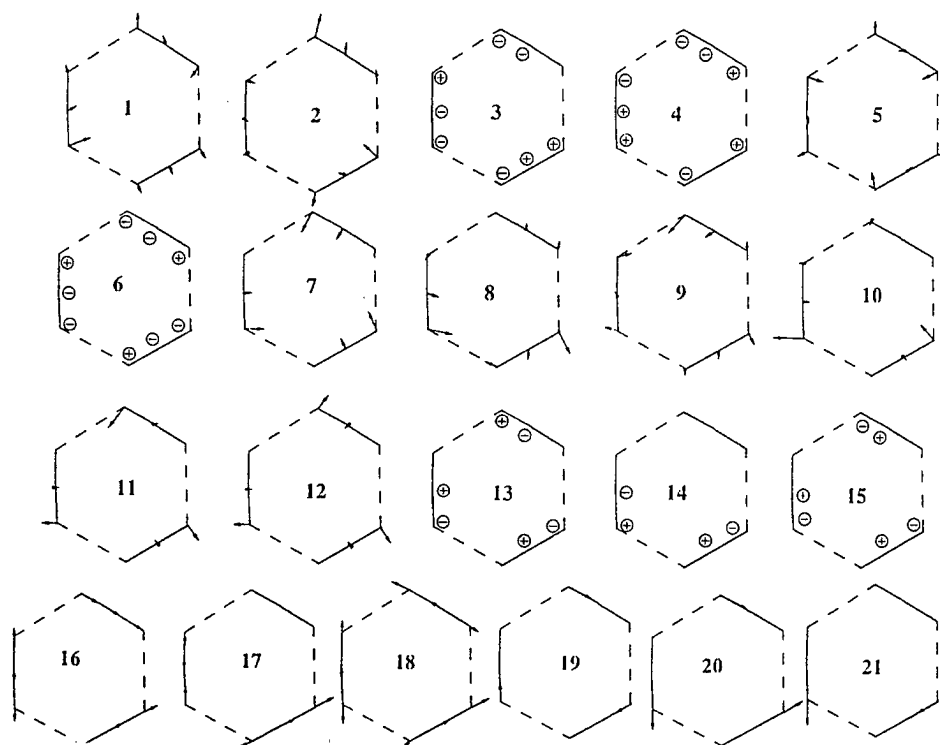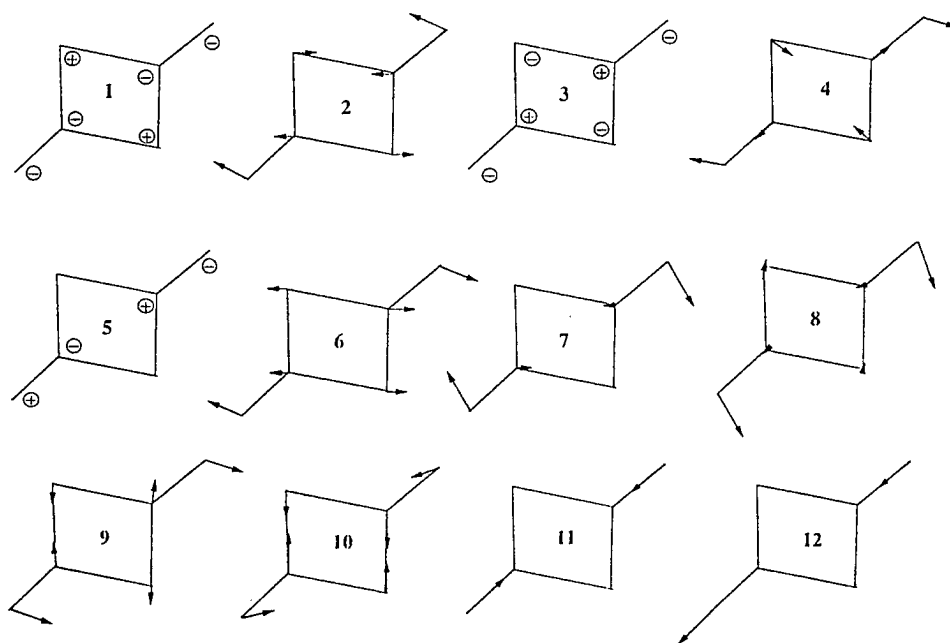
Figure 5. MP2/cc-pVTZ eigenvectors corresponding to harmonic vibrational frequencies (given in Table 2) for the (HCN)₃ cluster. Positive and negative signs denote out-of-plane motion.

Figure 6. MP2/cc-pVTZ eigenvectors corresponding to harmonic vibrational frequencies (given in Table 2) for the H₂C₂N₂ dimer. Positive and negative signs denote out-of-plane motion.
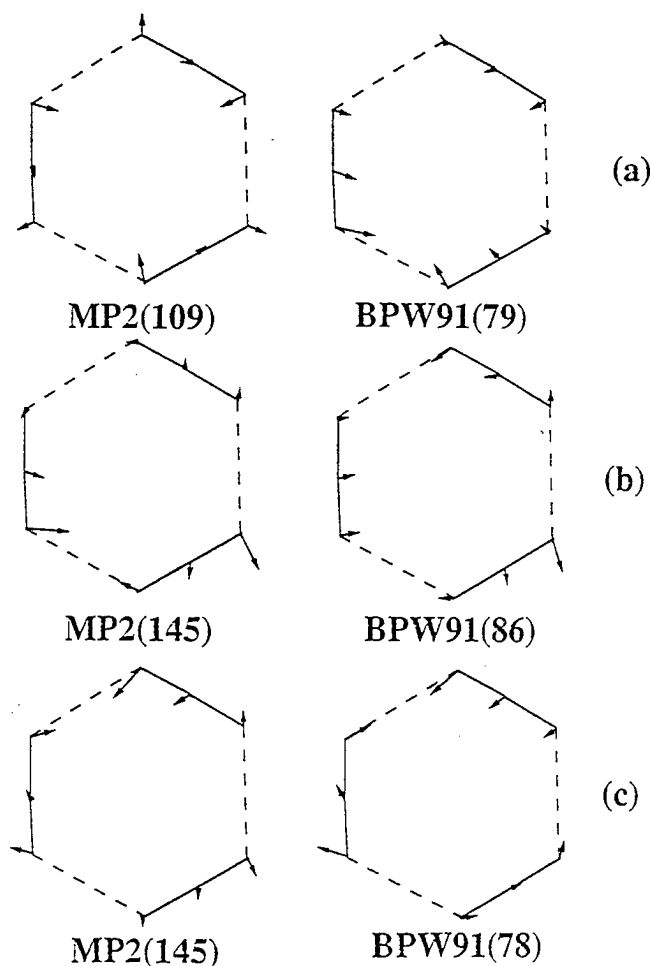
Figure 7. Comparison of MP2 eigenvectors to BPW91/cc-VTZ eigenvectors for (a) mode 5, (b) mode 8, and (c) mode 9 of the $(HCN)_3$ cluster.

eigenvectors correspond to modes 5, 8, and 9 (See Table 2.) It is clear that there are significant differences between the BPW91 and MP2 eigenvectors. The assignments we made that are listed in Table 2 are based solely on the combinations that provided the largest projection value of the eigenvectors. For the MP2 and BPW91 pairs shown in Figure 7, the projections of the BPW91 onto the MP2 are 0.41, 0.74, and 0.72, respectively.

In order to compare effects of basis sets and methods on the harmonic vibrational frequencies, we calculated the difference of the prediction with some standard. In the case of basis set size dependence, the standards are the cc-pVTZ calculations. For determination of the effect of the theoretical method, the standard is experiment, where available, and MP2 theory where experimental data do not exist.

14

The theoretical frequencies neglect anharmonicity, therefore, the best theoretical calculations should in principle lie above the exact experimental frequencies. Simply because one theoretical technique lies closer to the exact experimental value than another does not necessarily mean that this method is a better reproduction of the vibrational modes.

3.2.1 Basis Set Size Dependence. The differences in harmonic frequencies calculated using the 6-31G** and 6-311++G** basis sets relative to those calculated using the cc-pVTZ basis set are given in parentheses within the columns in Table 2 labeled "6-31G**" and "6-311++G**". DFT predictions of frequencies of the critical points have small basis set dependencies. Increasing the basis set from 6-31G** to 6-311++G** brings most modes to within ~10 cm^{-1} of the cc-pVTZ predictions for all species; no frequency differs by more than 25 cm^{-1}. In contrast, the MP2 predictions of harmonic vibrational frequencies show significant basis set dependencies, and some 6-311++G** frequencies are in significantly poorer agreement with cc-pVTZ than the 6-31G** values.

3.2.2 Method Comparison. Figure 8 provides a comparison of predicted harmonic vibrational frequencies using the cc-pVTZ basis set with experiment for HCN and *sym*-triazine. Figure 9 compares DFT-harmonic vibrational frequencies with MP2/cc-pVTZ frequencies for the transition state, the (HCN)$_3$ cluster, and the dimer.

For HCN and *sym*-triazine, BPW91, BP86, and BLYP provide best overall agreement with experiment [to within 50 cm^{-1} for all modes except for *sym*-triazine modes 13 [(1251 cm^{-1})] and 18 [(1617 cm^{-1})]. However, modes 13 and 18 correspond to two A$'_2$ fundamentals which are inactive and not observed. The values for these fundamentals given in the experimental paper are from "estimated force constants and hence are only very approximate" (Lancaster, Stamm, and Colthup 1961). MP2 agrees with the experimental value given for *sym*-triazine mode 13 to within 8 cm^{-1}. However, the good agreement could be fortuitous. MP2 and B3LYP predictions for all HCN and *sym*-triazine modes with energies less than 2000 cm^{-1} (except for mode 18, discussed previously) agree with experiment to within 50 cm^{-1}; agreement with modes of higher energy is not as good.

All DFT-frequency predictions for the transition state, the (HCN)$_3$ cluster, and the dimer are within 200 cm^{-1} of the MP2 predictions. For bound modes up to 1300 cm^{-1}, all DFT predictions are within 100 cm^{-1} of the MP2 values. B3LYP provides the best agreement with MP2 for the transition state and the dimer. BLYP gives the best agreement with MP2 for the (HCN)$_3$ cluster.
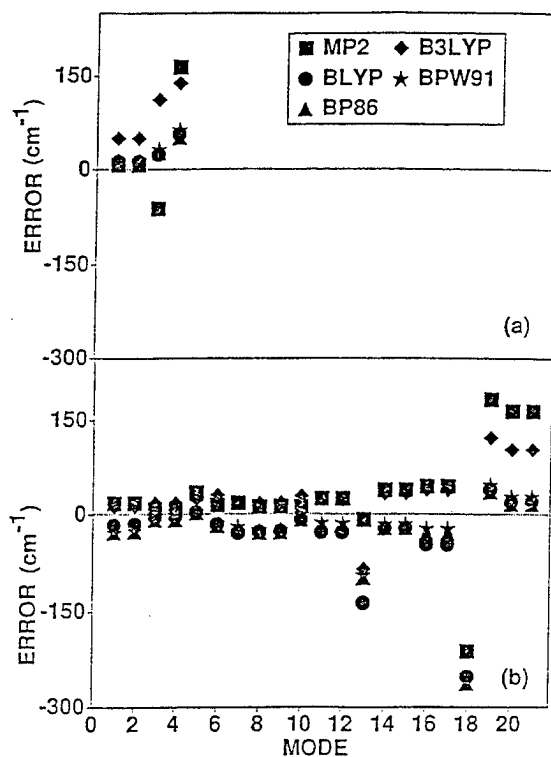
15

Figure 8. Error from experiment for the harmonic vibrational frequencies of (a) HCN and (b) *sym*-triazine for all methods using the cc-pVTZ basis set. Method is denoted by symbols in the legend in Figure 8(a).
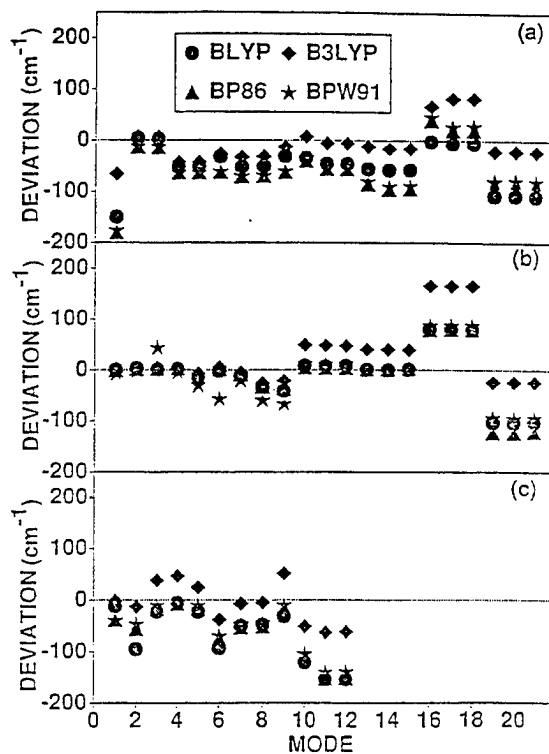

Figure 9. Difference in DFT/cc-pVTZ frequencies from MP2/cc-pVTZ for (a) the transition state, (b) the (HCN)$_3$ cluster, and (c) the H$_2$C$_2$N$_2$ dimer. Method is denoted by symbols in the legend in Figure 9(a).

16

A single vibration of the $(HCN)_3$ cluster has been measured and assigned as the doubly degenerate C-H asymmetric stretch (Jucks and Miller 1988). The vibrational frequency is 3274 cm^{-1} and contains rotationally resolved bands (Jucks and Miller 1988). DFT predictions of the frequency of this vibrational mode are in closer agreement to experiment than MP2. BP86 provides the closest agreement and is 1.3% larger than the experiment. Fits of the bands to rotational transitions assuming a planar oblate symmetric top result in rotational constants A"=B"=2C"=0.0822 cm^{-1} (Jucks and Miller 1988). DFT predictions of the rotational constant deviate from experiment by 1–6%, with BP86 and B3LYP having the best agreement with experiment (0.0814 and 0.0815 cm^{-1}, respectively). MP2/cc-pVTZ predictions are within 2% (0.0840 cm^{-1}) and BLYP and BPW91 predictions are 0.0791 and 0.0770 cm^{-1}, respectively.

The projection of DFT eigenvectors onto the MP2 eigenvectors is not used only to assign vibrational modes. The magnitude of the projections of the DFT eigenvectors onto the MP2 eigenvectors is a measure of the agreement in the description of the atomic motions of the molecules for each vibration. A projection that has a magnitude of approximately one indicates similarity in the DFT and MP2 predictions of atomic motions of the molecule corresponding to that vibrational mode. A projection that has a magnitude near zero indicates that the two theoretical methods describe significantly differently the motions for that vibration.

Since the details of atomic motions corresponding to each normal mode of vibration cannot be determined through experiment without assuming some sort of model (as in the experimental work on *sym*-triazine) (Vosko, Wilk, and Nusair 1980), we have used the MP2 eigenvectors as the standard against which to compare the goodness of the DFT predictions.

Figure 10 shows the projection of the DFT/cc-pVTZ eigenvectors onto MP2/cc-pVTZ eigenvectors corresponding to vibrational modes for *sym*-triazine, the transition state, the $(HCN)_3$ cluster, and the dimer. The eigenvectors have little dependence on the quality of the basis set for all of the critical points on the PES. DFT eigenvectors of *sym*-triazine are in excellent agreement with MP2 predictions except for degenerate modes 3–4, 16–17, and 20–21 [Figure 10(a)].

This lesser agreement between the DFT and MP2 eigenvectors for these pairs of degenerate modes is probably due to the nonuniqueness of the eigenvectors for each degenerate pair which arises from the three-fold rotational symmetry of the molecule. Such a comparison for degenerate modes is valid only if some attempt is made to rotate the degenerate DFT eigenvectors so as to maximize their agreement with
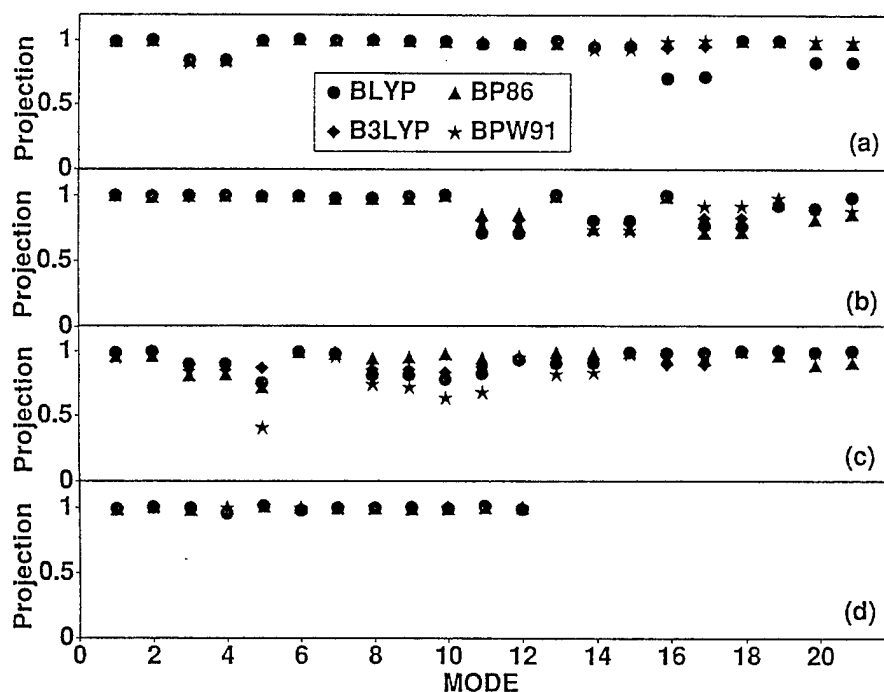
Figure 10. Projection of DFT/cc-pVTZ eigenvectors corresponding to harmonic frequencies onto MP2/cc-pVTZ eigenvectors for (a) *sym*-triazine, (b) the transition state for Reaction (I), (c) the (HCN)$_3$ cluster, and (d) the H$_2$C$_2$N$_2$ dimer. Symbols in the legend shown in Figure 10(a) denote the method.

the MP2 eigenvectors. Due to the good agreement with the nondegenerate modes, we assumed that the lack of exact agreement for these modes is most likely an artifact of the "nonuniqueness" of the eigenvectors for these double degenerate modes rather than any differences in the predictive quality of either theory. Thus, we did not attempt to rotate the degenerate DFT eigenvectors into coincidence with the MP2 eigenvectors. Excluding the degenerate modes, all of the DFT predictions are in equally good agreement with the MP2 vibrational eigenvectors of *sym*-triazine.

Excellent agreement exists among all DFT and MP2 calculations for modes 1–10 of the transition state [Figure 10(b)] as evidenced by the magnitude of the DFT projections for those modes. However, the magnitudes of the projections for the higher frequency modes of the transition state are not as large, and have values as low as 0.7. In those cases, the atomic motions predicted by DFT for those vibrational modes are not the same as the MP2 predictions, although the DFT frequencies are within 10% of the MP2 values. Conversely, the DFT predictions of the imaginary frequency of the transition state ranged from 10 to 30% disagreement with the MP2 value while the magnitude of the projections of the DFT eigenvectors on the MP2 eigenvector for this mode are all ~1. It appears that all of the DFT methods perform equally well in predicting the vibrational eigenvectors for the transition state.

18

For the $(HCN)_3$ cluster, the BP86 eigenvectors have the largest projections onto the MP2 eigenvectors [Figure 10(c)] over the entire spectrum. Significant scatter exists in the projections for the remaining methods, with BPW91 showing the most notable disagreement with MP2 (see Figure 7 and previous discussion). Finally, for the dimer, all DFT eigenvectors project almost equally well onto the MP2 eigenvectors over the entire spectrum [Figure 10(d)].

3.3 **IRC.** Figure 11 shows DFT/6-31G** and MP2/6-31G** energies along the reaction coordinate for concerted triple decomposition of *sym*-triazine [Reaction (I)]. Figure 12 shows corresponding geometric parameters along the path. The energies in Figure 11 are relative to three isolated HCN molecules. Zero-point corrections are not included in Figure 11. The *sym*-triazine minimum is located on the right side of Figure 11, and the $(HCN)_3$ cluster minimum is on the left-hand side. Although we conducted a thorough search, we were unable to find a transition state connecting minima for the $(HCN)_3$ cluster and isolated HCN molecules.
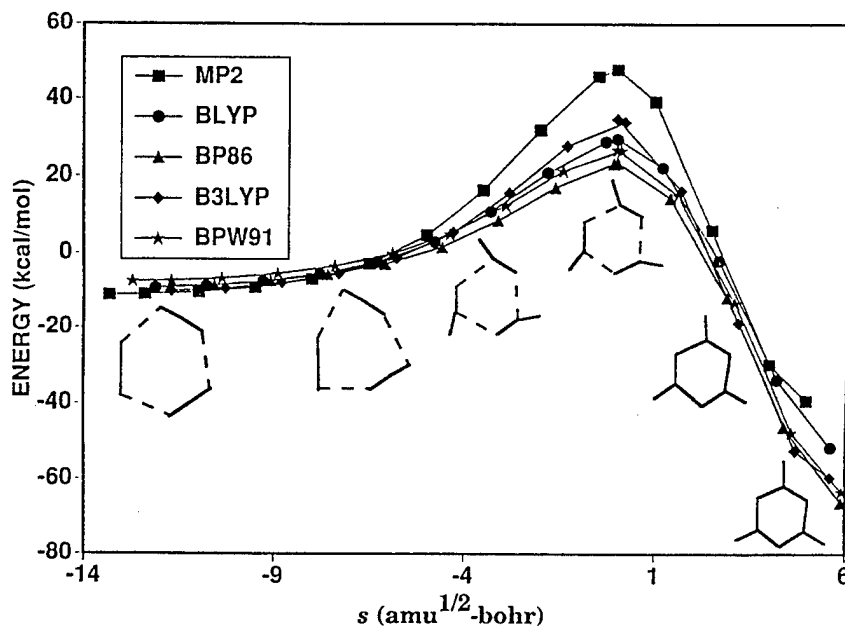

Figure 11. <u>Energies along the reaction path for Reaction (I) determined from IRC/6-31G** calculations using all methods.</u> Every tenth point along the reaction path from the IRC calculations is shown. In addition to the $(HCN)_3$ cluster (illustrated at the leftmost portion of this figure), the transition state structure, and *sym*-triazine (illustrated at the rightmost portion of the figure), three additional structures along the reaction path have been shown to enable the reader to visualize the mechanism of concerted dissociation of *sym*-triazine. The method is denoted by the symbols defined in the legend. Energy is relative to three isolated HCN molecules.
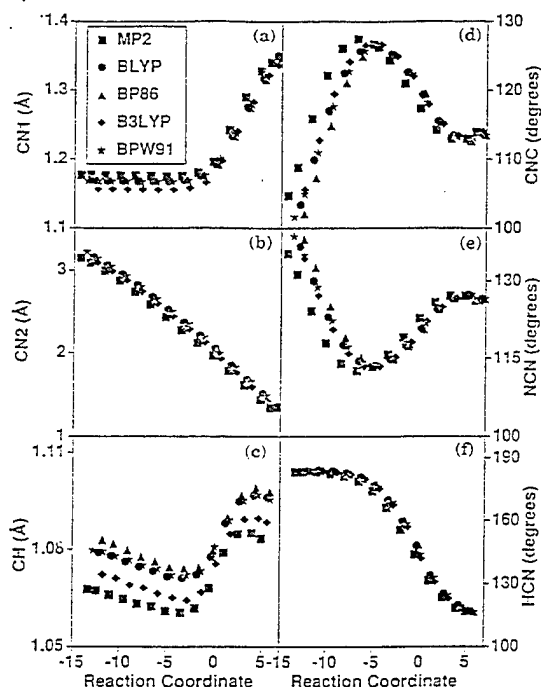
19

Figure 12. **Internal coordinate changes along the reaction path for Reaction (I).** See Figure 1(b) for the definition of internal coordinates. Bond lengths are in Å and bond angles are in degrees. The reaction coordinate is in mass-weighted units of $amu^{1/2}$-bohr. Method is denoted by the symbols defined in the legend.

The energy profiles of the reaction paths calculated by all the methods have the same shape but differ in the magnitude of the barrier and relative well depths of *sym*-triazine and the $(HCN)_3$ cluster. B3LYP/6-31G** predicts the largest classical barrier to decomposition of *sym*-triazine (94.1 kcal/mol), and BLYP/6-31G** predicts the smallest (81.0 kcal/mol). The BP86 and BPW91 values (89.6 and 90.2 kcal/mol, respectively) are within 3 kcal/mol of the MP2/6-31G** prediction (87.2 kcal/mol). For the reverse reaction, the association of three HCN molecules to form *sym*-triazine, MP2 predicts the largest classical barrier (47.4 kcal/mol) and BP86 predicts the smallest (23.3 kcal/mol).

Our calculations indicate that the structures maintain three-fold symmetry throughout the reaction path, as can be seen in the series of snapshots of the atoms at points along the reaction path shown in Figure 11. The changes in internal coordinates for all methods, illustrated in Figure 12, are quantitatively similar. Therefore, DFT predictions of geometric changes along the reaction path are as good as MP2, and energy profiles are in qualitative agreement with MP2.

3.4 Energetics. Table 3 lists the DFT and *ab initio* absolute and relative energies, and Table 4 lists DFT and *ab initio* energy differences of critical points (zero point corrected) on the potential energy surface for *sym*-triazine reactions. The deviation of energy differences calculated using the 6-31G** or

Table 3. Absolute Energies (Hartrees) of Species on the *sym*-Triazine Potential Energy Surface

Level	Basis Set	3HCN	3HCN--> *sym*-triazine transition state	*sym*-triazine	(HCN)$_3$	H$_2$C$_2$N$_2$+HCN
MP2[a]	6-31G**	-279.4985190	-279.4225671	-279.5614678	-279.5162594	-279.4040450
QCISD(T)//MP2[a]	6-31G**	-279.5589918	-279.4839155	-279.6242656	-279.5758546	-279.4746539
BLYP	6-31G**	-280.2052059	-280.1584086	-280.2875065	-280.2200309	-280.1290241
BP86	6-31G**	-280.2685965	-280.2314424	-280.3742006	-280.2827112	-280.2062887
B3LYP	6-31G**	-280.2737445	-280.2187381	-280.3687292	-280.2901841	-280.2000628
BPW91	6-31G**	-280.2437313	-280.2012304	-280.3449176	-280.2555965	-280.1798293
MP2[a]	6-311++G**	-279.6096735	-279.5319344	-279.6661137	-279.6262566	-279.5142543
QCISD(T)//MP2[a]	6-311++G**	-279.6717324	-279.5945901	-279.7308072	-279.6877556	-279.5865234
BLYP	6-311++G**	-280.3028328	-280.2448079	-280.3637926	-280.3139501	-280.2155600
BP86	6-311++G**	-280.3555890	-280.3107444	-280.4446191	-280.3669224	-280.2848093
B3LYP	6-311++G**	-280.3635150	-280.2989407	-280.4392736	-280.3769038	-280.2799188
BPW91	6-311++G**	-280.3286481	-280.2786145	-280.4138659	-280.3379973	-280.2566598
MP2[a]	cc-pVTZ	-279.7607679	-279.6923459	-279.8296494	-279.7782811	-279.6699089
QCISD(T)//MP2[a]	cc-pVTZ	-279.8271414	-279.7566438	-279.8963920	-279.8436781	-279.7449569
BLYP	cc-pVTZ	-280.3211079	-280.2642618	-280.3839139	-280.3332164	-280.2334668
BP86	cc-pVTZ	-280.3742580	-280.3302634	-280.4648116	-280.3860816	-280.3033059
B3LYP	cc-pVTZ	-280.3841184	-280.3206284	-280.4618104	-280.3981260	-280.3003421
BPW91	cc-pVTZ	-280.3478544	-280.2985789	-280.4344963	-280.3576338	-280.2756938

Relative energies (kcal/mol) of species on the *sym*-triazine potential energy surface

Level	Basis Set	3 HCN	3 HCN--> *sym*-triazine transition state	*sym*-triazine	(HCN)$_3$	H$_2$C$_2$N$_2$+HCN
MP2[a]	6-31G**	0.0	47.7	-39.5	-11.1	59.3
QCISD(T)//MP2[a]	6-31G**	0.0	47.1	-41.0	-10.6	52.9
BLYP	6-31G**	0.0	29.4	-51.6	-9.3	47.8
BP86	6-31G**	0.0	23.3	-66.3	-8.9	39.1
B3LYP	6-31G**	0.0	34.5	-59.6	-10.3	46.2
BPW91	6-31G**	0.0	26.7	-63.5	-7.4	40.1
MP2	6-311++G**	0.0	48.8	-35.4	-10.4	59.9
QCISD(T)//MP2[a]	6-311++G**	0.0	48.4	-37.1	-10.1	53.5
BLYP	6-311++G**	0.0	36.4	-38.3	-7.0	54.8
BP86	6-311++G**	0.0	28.1	-55.9	-7.1	44.4
B3LYP	6-311++G**	0.0	40.5	-47.5	-8.4	52.5
BPW91	6-311++G**	0.0	31.4	-53.5	-5.9	45.2
MP2	cc-pVTZ	0.0	42.9	-43.2	-11.0	57.0
QCISD(T)//MP2[a]	cc-pVTZ	0.0	44.2	-43.5	-10.4	51.6
BLYP	cc-pVTZ	0.0	35.7	-39.4	-7.6	55.0
BP86	cc-pVTZ	0.0	27.6	-56.8	-7.4	44.5
B3LYP	cc-pVTZ	0.0	39.8	-48.8	-8.8	52.6
BPW91	cc-pVTZ	0.0	30.9	-54.4	-6.1	45.3

[a] Pai, Chabalowski, and Rice (1996).

Table 4. Zero-Point Corrected Energy Differences (kcal/mol) on the *sym*-Triazine Potential Energy Surface

Method	ΔE (Transition State—3HCN)			ΔE (*sym*-triazine—3HCN)			ΔE (Transition State—*sym*-triazine)			ΔE [(HCN)₃—3HCN]			ΔE [(H₂C₂N₂ + HCN)—3HCN]		
	6-31G**	6-311++G**	cc-pVTZ	6-31G**	6-311++G**	cc-pVTZ	6-31G**	6-311++G**	cc-pVTZ	6-31G**	6-311++G**	cc-pVTZ	6-31G**	6-311++G**	cc-pVTZ
MP2[a]	52.8 (4.9)	53.2 (5.3)	47.9	-27.9 (3.8)	-24.5 (7.2)	-31.7	80.7 (1.0)	77.7 (-2.0)	79.7	-9.4 (0.1)	-9.2 (0.3)	-9.5	63.8 (2.5)	64.0 (2.7)	61.3
QCISD(T)[a]	52.2 (3.0)	52.8 (3.6)	49.2	-29.4 (2.6)	-26.2 (5.8)	-32.0	81.6 (0.4)	79.0 (-2.2)	81.2	-8.9 (0.0)	-8.9 (0.0)	-8.9	57.4 (1.5)	57.6 (1.7)	55.9
BLYP	32.7 (-6.7)	40.0 (0.6)	39.4	-42.1 (-12.4)	-28.7 (1.0)	-29.7	74.8 (5.7)	68.7 (-0.4)	69.1	-7.9 (-1.6)	-5.7 (0.6)	-6.3	50.9 (-7.3)	58.0 (-0.2)	58.2
BP86	26.5 (-4.6)	31.6 (0.5)	31.1	-56.7 (-9.6)	-46.2 (0.9)	-47.1	83.2 (5.0)	77.8 (-0.4)	78.2	-7.5 (-1.4)	-5.8 (0.3)	-6.1	42.3 (-5.5)	47.7 (-0.1)	47.8
B3LYP	38.2 (-5.3)	44.1 (0.6)	43.5	-49.4 (-10.6)	-37.6 (1.2)	-38.8	87.6 (5.3)	81.8 (-0.5)	82.3	-8.6 (-1.1)	-7.1 (0.4)	-7.5	49.7 (-6.3)	55.9 (-0.1)	56.0
BPW91	30.1 (-4.4)	34.7 (0.2)	34.5	-53.7 (-9.2)	-43.9 (0.6)	-44.5	83.8 (4.8)	78.6 (-0.4)	79.0	-6.0 (-1.2)	-4.9 (-0.1)	-4.8	43.4 (-5.3)	48.4 (-0.3)	48.7

[a]Pai, Chabalowski, and Rice (1996).

6-311++G** basis sets from those calculated using the cc-pVTZ basis set are given in parentheses within the columns in Table 4 labeled "6-31G**" and "6-311++G**." Figure 13 is an energy-level diagram based on the values given in Table 4. This diagram illustrates the two assumed decomposition mechanisms for *sym*-triazine. The minimum for the isolated HCN molecules is located at the center of the figure and is labeled "3 HCN." Critical points to the left of this minimum represent features along the step-wise decomposition pathway [Reaction (II)]. Critical points to the right of the minimum labeled "3 HCN" represent features along the concerted triple-decomposition pathway [Reaction (I)].

3.4.1 Basis Set Size Dependence. Except for the energy difference between isolated HCN and the $(HCN)_3$ cluster, DFT/6-31G** values differ from the DFT/cc-pVTZ values by 4.4–12.4 kcal/mol. The DFT/6-311++G** differences, however, are within 1.2 kcal/mol of the DFT/cc-pVTZ differences. For the reaction barriers, the differences between DFT/6-311++G** and DFT/cc-pVTZ are no greater than 0.6 kcal/mol. While both the 6-311++G** and the cc-pVTZ basis sets are considered triple zeta in the valence space, one very significant difference between them is in the number of polarization functions in each set. For hydrogen, the former has a single-primitive p-type polarization function, and a single-primitive d-type on the first-row atoms. The cc-pVTZ has two p-type and one d-type function on hydrogen, while the first-row atoms have two d-type and one f-type polarization functions, where all are single uncontracted primitive functions. The DFT results show very little dependence on the quality of the basis set used to define the polarization space. Except for the energy difference between the isolated HCN molecules and the $(HCN)_3$ cluster, *ab initio*/6-311++G** values are in poorer agreement with the cc-pVTZ values than the 6-31G** values. For the *ab initio* calculations, one would expect the polarization functions to play a significant role in correcting correlation error (Woon and Dunning 1993; Kendall, Dunning, and Harrison 1992; Dunning 1989) and that seems to be the case here. In contrast, the current study shows the DFT results to have very little dependence on the polarization functions.

3.4.2 Method Comparison. The zero-point corrected energies of $H_2C_2N_2$ + HCN relative to three isolated HCN molecules are higher than the zero-point corrected relative energy of the transition state for Reaction (I) for all methods and with all basis sets. Focusing only on the cc-pVTZ basis, the QCISD(T)//MP2 predicts that the $H_2C_2N_2$ + HCN minimum is 6.7 kcal/mol higher than the transition state for concerted triple dissociation [Reaction (I)]. The DFT predictions of the $H_2C_2N_2$ + HCN minimum range from 12.5 to 18.8 kcal/mol higher than the barrier to concerted triple dissociation. Therefore, even if we assume that there are no barriers to formation of $H_2C_2N_2$ + HCN from *sym*-triazine decomposition
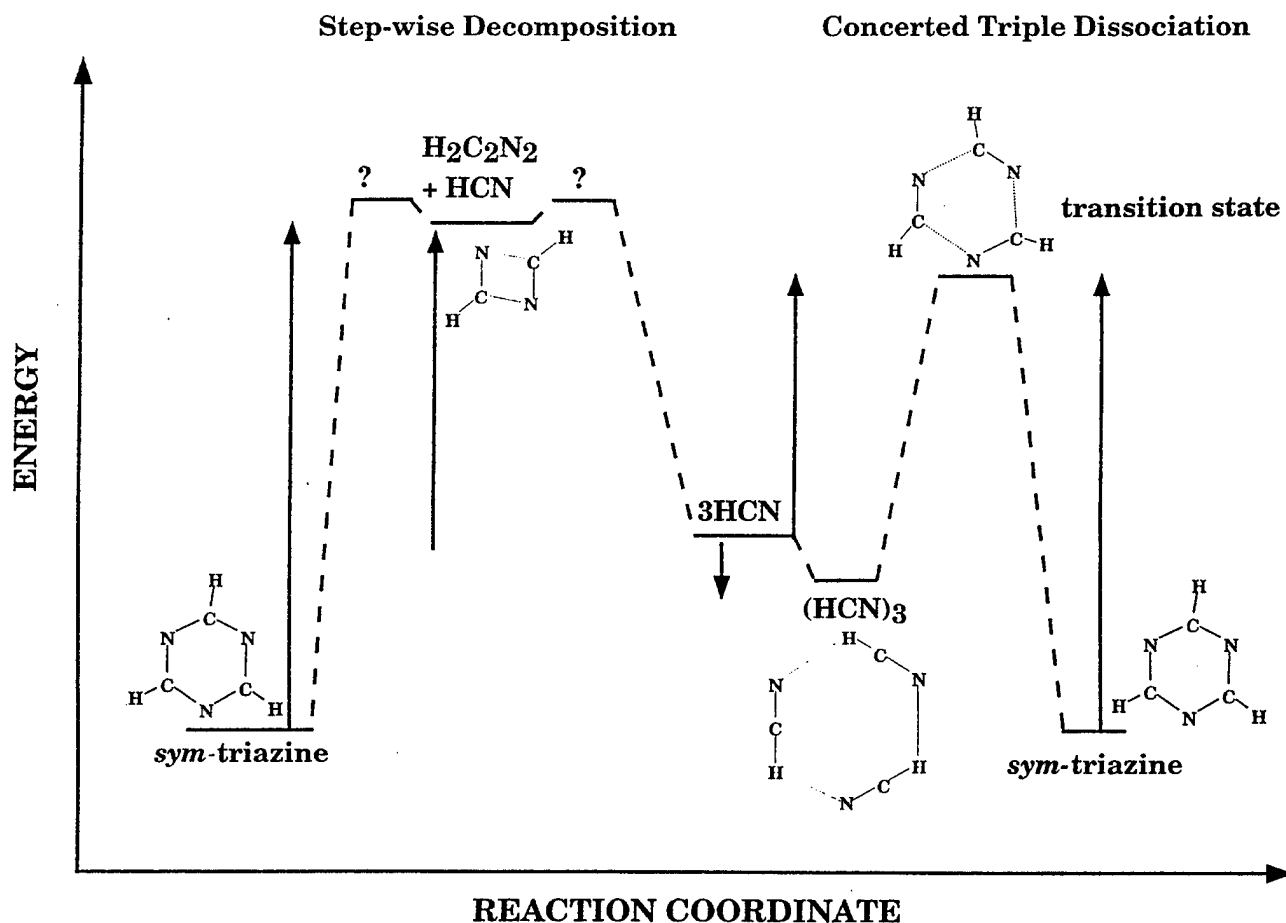
23

Figure 13. Energy-level diagram for the *sym*-triazine potential energy surface showing the minima and saddle point energies. Zero-point corrected energy differences between critical points using the different methods and the 6-31G**, 6-311++G**, and cc-pVTZ basis sets are given in Table 4. The diagram is representative of the features of the PES calculated with all methods, and is illustrative of points made in the text.

or from association of two HCN molecules [the reverse of Reaction (II)], the step-wise decomposition reaction will be higher in energy than the concerted triple decomposition. Our interests are mainly in the low-energy pathway for the decomposition reactions of *sym*-triazine; therefore, we did not investigate this step-wise reaction path any further. Two of the DFT methods (BPW91 and BP86) predict energies of the dimer minimum (relative to isolated HCN) that are at least 7.2 kcal/mol lower than the *ab initio* predictions. The remaining DFT methods are within 2.3 kcal/mol of the QCISD(T)//MP2 value.

The predictions of the well depths of the $(HCN)_3$ cluster relative to the isolated HCN molecules range from −4.8 to −9.5 kcal/mol using the largest basis set, with *ab initio* predicting deeper minima than DFT by at least 1.4 kcal/mol. The BPW91 prediction has the greatest disagreement with *ab initio* and is 4.1 kcal/mol higher in energy than the QCISD(T)//MP2 value. *Sym*-triazine shows the opposite trend,

where BP86, B3LYP, and BPW91 predict the relative well depth to be greater than that predicted by *ab initio* by at least 6.8 kcal/mol, and in the case of BP86 and BPW91, by 12–15 kcal/mol. BLYP prediction of the *sym*-triazine well depth is in closest agreement with the *ab initio* predictions, being higher by 2 kcal/mol.

With the exception of BLYP, the DFT/cc-pVTZ barrier heights for the concerted triple decomposition of *sym*-triazine are within 3 kcal/mol of the *ab initio* predictions. BPW91 and BP86 are within 1.5 kcal/mol of the MP2 values, and B3LYP is ~1 kcal/mol higher than the QCISD(T)//MP2 value. BLYP stands out by being significantly lower (by ~9–12 kcal/mol) than predictions using all other methods. The only experimental data for this barrier were obtained through photodissociation experiments, the results of which provided an upper limit of 115 kcal/mol (Ondrey and Bersohn 1984).

All DFT/cc-pVTZ predictions of the barrier height for the reverse reaction of (I), the concerted triple association of 3 HCN molecules to form *sym*-triazine, are lower than the *ab initio* predictions by at least 4 kcal/mol. The B3LYP result is in closest agreement with *ab initio*; all other methods underestimate the *ab initio* values by at least 8.5 kcal/mol.

The measured endothermicity of Reaction (I) is 43.2 kcal/mol (Ondrey and Bersohn 1984). Figure 14 compares temperature-corrected (T = 298 K) reaction enthalpies for *sym*-triazine decomposition calculated by all the methods using the cc-pVTZ basis set. The B3LYP prediction has the best agreement with experiment (42.1 kcal/mol), followed by BPW91 (48 kcal/mol). BP86 predicts a larger reaction enthalpy (50.4 kcal/mol), and BLYP significantly underestimates the experiment (33.1 kcal/mol). MP2 and subsequent QCISD(T) refinements predict reaction enthalpies of 35.2 and 34.4 kcal/mol, substantially smaller than the experiment, and in almost as poor agreement as BLYP. This indicates clearly that B3LYP predictions of the reaction enthalpy for this system are superior to *ab initio*.

4. CONCLUSIONS

In this study, we have compared the performance of NDFT (BP86, BLYP, B3LYP, and BPW91) using three basis sets (6-31G**, 6-311++G**, and cc-pVTZ) with *ab initio* methods [MP2 and QCISD(T)] and experiment, where available, for predicting molecular properties at critical points along two decomposition reaction pathways of *sym*-triazine. The two decomposition pathways that are investigated are a concerted triple dissociation and a step-wise decomposition involving an $H_2C_2N_2$ intermediate. DFT and *ab initio*

25

sym-triazine —> 3HCN

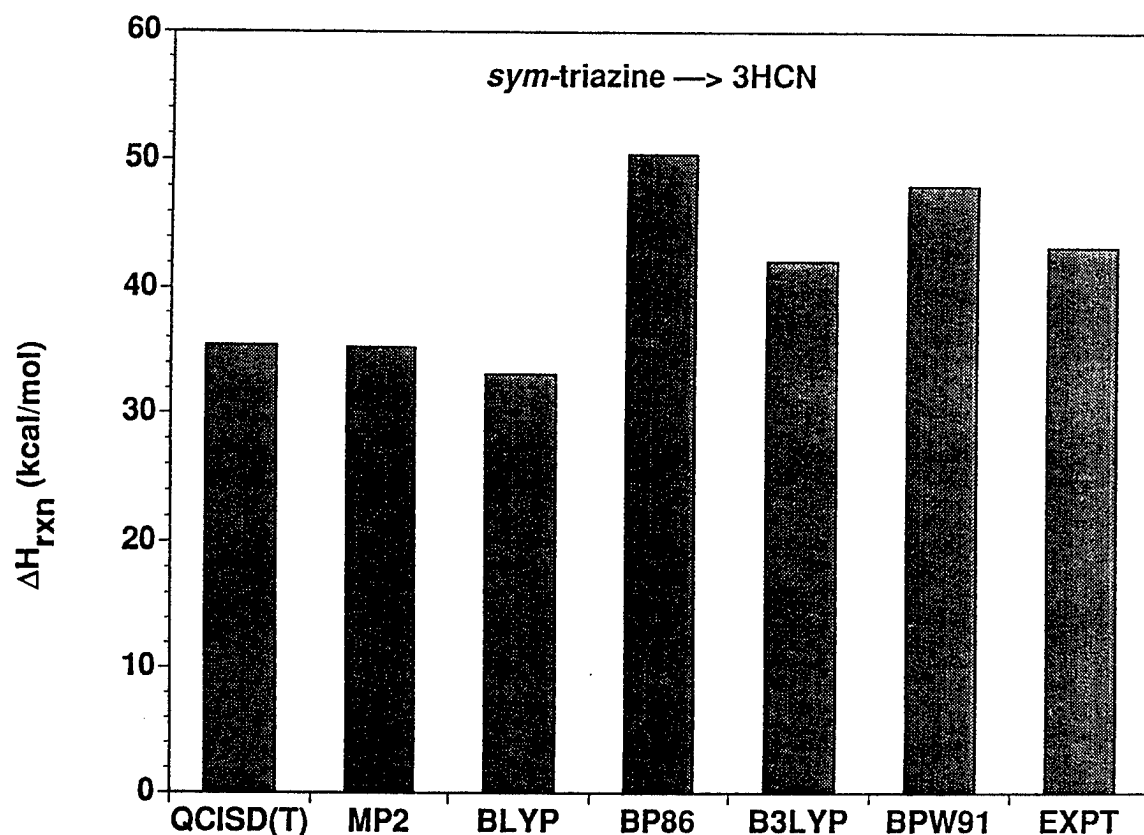Figure 14. Temperature-corrected (T=298 K) reaction enthalpies for Reaction (I). The quantum mechanical method is labeled along the abscissa; all calculations used the cc-pVTZ basis set. The experimental value is given in Ondrey and Bersohn (1984).

geometries, harmonic vibrational frequencies, and corresponding eigenvectors, and relative energies of critical points were compared. Additionally, energies and structures were compared along the IRC for the triple-concerted decomposition of sym-triazine using the 6-31G** basis set. All methods predict that the low-energy pathway to decomposition of sym-triazine is a concerted triple dissociation, and that a weakly bound cyclic $(HCN)_3$ cluster exists on the reaction path. All methods predict that three-fold symmetry is maintained at all points along the reaction coordinate. The energy profile along the reaction coordinate is qualitatively similar for all methods; the main differences are in the sizes of the reaction barriers and the well depths of sym-triazine relative to three isolated HCN molecules.

We find that increasing the basis set size does not significantly affect the prediction of structural parameters for all methods. Geometries of sym-triazine and HCN predicted by all methods and for all basis sets are within 2% of experiment. DFT/cc-pVTZ predictions of the geometries of the transition state,

the $(HCN)_3$ cluster, and the $H_2C_2N_2$ dimer are in good agreement with the MP2 predictions. The largest disagreement between the DFT/cc-pVTZ and MP2/cc-pVTZ structures is <7%.

The frequencies of the structures on this PES show small basis set size dependence for all methods. The majority of DFT vibrational frequencies calculated using the 6-311++G** basis set are within 10 cm^{-1} of the cc-pVTZ values. BPW91, BP86, and BLYP predictions of the vibrational frequencies of HCN and *sym*-triazine are within 50 cm^{-1} of all experimentally observed modes. MP2 and B3LYP predictions perform as well as the other DFT methods for modes with energies <2000 cm^{-1}. All DFT/cc-pVTZ predictions of harmonic vibrational frequencies for the transition state, the $(HCN)_3$ cluster, and the dimer are within 200 cm^{-1} of MP2 predictions for all modes and within 100 cm^{-1} for modes with energies less than 1300 cm^{-1}. Very little, if any, experimental data exist for the transition state species, the $(HCN)_3$ cluster, and the dimer. If we then assume the MP2 results to be correct, there appears to be no one set of functionals that stands out as consistently predicting frequencies in better agreement with MP2 than the other functionals. Therefore, we cannot conclude that one functional better describes these species than another.

The projection of the DFT/cc-pVTZ eigenvectors onto MP2/cc-pVTZ eigenvectors shows that for most modes of *sym*-triazine and all modes of the dimer, the DFT eigenvectors are quantitatively similar to the MP2 eigenvectors. For noncovalently bound species [the transition state and the $(HCN)_3$ cluster], the DFT results show poorer agreement with MP2 eigenvectors, with no obvious relationship between the degree of agreement and specific regions in the spectrum. In particular, the poor agreement between MP2 and DFT (especially BPW91) eigenvectors for a few low-frequency modes of the $(HCN)_3$ cluster and a few modes in the transition state suggests caution in theoretical treatments of species with bonds that are weak or have intermediate bonding character.

Concerning the energetics for this reaction, there are some general trends that appear in contrasting the DFT against the *ab initio* results. For the DFT results, essentially all of the basis set dependence is contained in the basis functions describing the valence shell, while the *ab initio* results seem to depend equally on improvements in both the valence and polarization bases. These trends are clearly shown in Table 4, where the largest change in any ΔE using DFT between the 6-311++G** and cc-pVTZ basis sets is only 1.2 kcal/mol, while the change in going from the double zeta 6-31G** to triple zeta 6-311++G** is as large as 13 kcal/mol. In contrast, for the *ab initio* calculations in Table 4, the largest difference in any ΔE going from 6-31G** to 6-311++G** is about 3 kcal/mol, and going from 6-311++G** to

27

cc-pVTZ is ~7 kcal/mol. The valence and polarization functions appear to play an equally important role in the *ab initio* calculations, in contrast to the DFT where the polarization functions seem to play an essentially insignificant role. This shows that the polarization functions are crucial in the *ab initio* calculations for correcting the correlation errors present in the zeroth-order wave function through the perturbation theory, but in DFT the correlation is included in the zeroth-order density which is apparently adequately described by the valence shell basis set.

A comparison of the ΔE's for the transition states and energies of formation given in Table 4 show a wide scatter in the values predicted by the various density functionals. This is a noteworthy observation, since it provides evidence to the users of DFT that transition-state energies and energies of formation can be very dependent upon the choice of functionals. Fortunately, the qualitative features of the PES are the same regardless of the choice of functionals for this system. However, this serves as a warning that a quantitative prediction of a PES based upon DFT must be done after careful consideration of the choice of exchange and correlation functionals. To this end, if one assumes the QCISD(T) results to be the most accurate calculations in this study, it would appear that the B3LYP functionals give the most accurate DFT values for transition-state energies and energies of formation, with the exception of the zero-point corrected formation energy of *sym*-triazine from 3(HCN). The formation energy obtained from BLYP, −30 kcal/mol, lies closest to the QCISD(T) value of −32 kcal/mol, followed by the B3LYP value of −39 kcal/mol. This value, however, is closely related to the temperature-corrected reaction enthalpy for *sym*-triazine decomposition, which has been measured. The QCISD(T)-temperature-corrected reaction enthalpy is significantly smaller than the experimentally measured value of 43.2 kcal/mol (Ondrey and Bersohn 1984), whereas B3LYP is within 1.1 kcal/mol of the experiment. With this exception noted, for the set of functionals used in this study, the B3LYP appears to give the best overall agreement with the QCISD(T) results for ΔE's corresponding to transition states and energies of formation.

5. REFERENCES

Andzelm, J., C. Sosa, and R. A. Eades. Journal of Physical Chemistry, vol. 97, p. 4664, 1993.

Baker, J., J. Andzelm, M. Muir, and P. R. Taylor. Chemical Physics Letters, vol. 237, p. 53, 1995.

Becke, A. D. Physical Review A, vol. 38, p. 3098, 1988.

Becke, A. D. Journal of Chemical Physics, vol. 98, p. 5648, 1993.

Broclawik, E., H. Himei, M. Yamadaya, M. Kubo, and A. Miyamoto. Journal of Chemical Physics, vol. 103, p. 2102, 1995.

Deng, L., and T. Zeigler. Journal of Physical Chemistry, vol. 99, p. 612, 1995.

Deng, L., V. Branchadell, and T. Zeigler. Journal of the American Chemistry Society, vol. 116, p. 10645, 1994.

Dunning, T. H., Jr. Journal of Chemical Physics, vol. 90, p. 1007, 1989.

Fan, L., and T. Zeigler. Journal of Chemical Physics, vol. 92, p. 3645, 1990.

Fan, L., and T. Zeigler. Journal of the American Chemistry Society, vol. 114, p. 10890, 1992.

Frisch, M. J., G. W. Trucks, H. B. Schlegel, P. M. W. Gill, B. G. Johnson, M. A. Robb, J. R. Cheeseman, T. Keith, G. A. Petersson, J. A. Montgomery, K. Raghavachari, M. A. Al-Laham, V. G. Zakrzewski, J. V. Ortiz, J. B. Foresman, J. Cioslowski, B. B. Stefanov, A. Nanayakkara, M. Challacombe, C. Y. Peng, P. Y. Ayala, W. Chen, M. W. Wong, J. L. Andres, E. S. Replogle, R. Gomperts, R. L. Martin, D. J. Fox, J. S. Binkley, D. J. Defrees, J. Baker, J. P. Stewart, M. Head-Gordon, C. Gonzalez, and J. A. Pople. "Gaussian 94, Revision B.1." Gaussian, Inc., Pittsburgh, PA, 1995.

Gordon, M. S. Chemical Physics Letters, vol. 76, p. 163, 1980.

Hariharan, P. C., and J. A. Pople. Theoretica Chimica Acta, vol. 28, p. 213, 1973.

Hehre, W. J., R. Ditchfield, and J. A. Pople. Journal of Chemical Physics, vol. 56, p. 2257, 1972.

Hehre, W. J., L. Radom, P. Chleyer, and J. A. Pople. Ab Initio Molecular Orbital Theory. New York: Wiley, 1986.

Herzberg, G. Infrared and Raman Spectra of Polyatomic Molecules. Princeton, NJ: Van Nostrand, 1945.

Hohenberg, P., and W. Kohn. Physical Review B, vol. 136, p. 864, 1964.

Huber, K. P., and G. Herzberg. Constants of Diatomic Molecules. New York: Van Nostrand Reinhold, 1979.

Johnson, B. G., C. A. Gonzales, P. M. W. Gill, and J. A. Pople. Chemical Physics Letters, vol. 221, p. 100, 1994.

Jucks, K. W., and R. E. Miller. Journal of Chemical Physics, vol. 88, p. 2196, 1988.

Jursic, B. S. Journal of Organic Chemicals, vol. 60, p. 4721, 1995.

Kendall, R. A., T. H. Dunning, Jr., and R. J. Harrison. Journal of Chemical Physics, vol. 96, p. 6796, 1992.

Kohn, W., and L. J. Sham. Physical Review A, vol. 140, p. 113, 1965.

Krishnan, R., J. S. Binkley, R. Seeger, and J. A. Pople. Journal of Chemical Physics, vol. 72, p. 650, 1980.

Labanowski, J., and J. Andzelm (editors). Density Functional Methods in Chemistry. Berlin: Springer, 1991.

Lancaster, J. E., and B. P. Stoicheff. Canadian Journal of Physics, vol. 34, p. 1016, 1956.

Lancaster, J. E., R. F. Stamm, and N. B. Colthup. Spectrochimica Acta., vol. 17, p. 155, 1961.

Lee, C., W. Yang, and R. G. Parr. Physical Review B, vol. 37, p. 785, 1988.

McLean, A. D., and G. S. Chandler. Journal of Chemical Physics, vol. 72, p. 5639, 1980.

Miehlich, B., A. Savin, H. Stoll, and H. Preuss. Chemical Physics Letters, vol. 157, p. 200, 1989.

Moeller, C. M. S. Physical Review, vol. 46, p. 618, 1934.

Ondrey, G. S., and R. Bersohn. Journal of Chemical Physics, vol. 81, p. 4517, 1984.

Pai, S., C. Chabalowski, and B. Rice. Journal of Physical Chemistry, vol. 100, p. 5681, 1996.

Perdew, J. P. Physical Review B, vol. 33, p. 8822, 1986.

Perdew, J. P., and Y. Wang. Physical Review B, vol. 45, p. 13244, 1992.

Politzer, P., and J. M. Seminario (editors). Theoretical and Computational Chemistry. Amsterdam: Elsevier Scientific, vol. 1, 1995.

Porezag, D., and M. R. Pederson. Journal of Chemical Physics, vol. 102, p. 9345, 1995.

Schlegel, H. B. Adv. Chem. Phys., vol. 67, p. 249, 1987.

Sosa, C., and C. Lee. Journal of Chemical Physics, vol. 98, p. 8004, 1993.

Vosko, S. H., L. Wilk, and M. Nusair. Canadian Journal of Physics, vol. 58, p. 1200, 1980.

Woon, D. E., and T. H. Dunning, Jr. Journal of Chemical Physics, vol. 98, p. 1358, 1993.

Zeigler, T. Chemical Review, vol. 91, p. 651, and references therein, 1991.

NO. OF
COPIES ORGANIZATION

2 DEFENSE TECHNICAL INFO CTR
ATTN DTIC DDA
8725 JOHN J KINGMAN RD
STE 0944
FT BELVOIR VA 22060-6218

1 DIRECTOR
US ARMY RESEARCH LAB
ATTN AMSRL OP SD TA
2800 POWDER MILL RD
ADELPHI MD 20783-1145

3 DIRECTOR
US ARMY RESEARCH LAB
ATTN AMSRL OP SD TL
2800 POWDER MILL RD
ADELPHI MD 20783-1145

1 DIRECTOR
US ARMY RESEARCH LAB
ATTN AMSRL OP SD TP
2800 POWDER MILL RD
ADELPHI MD 20783-1145

ABERDEEN PROVING GROUND

2 DIR USARL
ATTN AMSRL OP AP L (305)

NO. OF COPIES	ORGANIZATION
1	AFOSR ATTN J M TISHKOFF BOLLING AIR FORCE BASE WASHINGTON DC 20332
1	OSD SDIO IST ATTN L CAVENY PENTAGON WASHINGTON DC 20301-7100
1	COMMANDANT USAFAS ATTN ATSF TSM CN FORT SILL OK 73503-5600
1	UNIV OF DAYTON RSRCH INST ATTN D CAMPBELL AL PAP EDWARDS AFB CA 93523
1	NASA LANGLEY RESEARCH CTR ATTN G B NORTHAM MS 168 LANGLEY STATION HAMPTON VA 23365
4	NATL BUREAU OF STANDARDS US DEPT OF COMMERCE ATTN J HASTIE M JACOX T KASHIWAGI H SEMERJIAN WASHINGTON DC 20234
2	DIRECTOR LAWRENCE LIVERMORE NATL LAB ATTN C WESTBROOK W TAO MS L 282 P O BOX 808 LIVERMORE CA 94550
1	DIRECTOR LOS ALAMOS NATL LAB ATTN B NICHOLS T7 MS B284 P O BOX 1663 LOS ALAMOS NM 87545

NO. OF COPIES	ORGANIZATION
2	PRINCETON COMBUSTION RESEARCH LABS INC ATTN N A MESSINA M SUMMERFIELD PRINCETON CORPORATE PLAZA BLDG IV SUITE 119 11 DEERPARK DRIVE MONMOUTH JUNCTION NJ 08852
3	DIRECTOR SANDIA NATL LABS DIVISION 8354 ATTN S JOHNSTON P MATTERN D STEPHENSON LIVERMORE CA 94550
1	BRIGHAM YOUNG UNIV DEPT OF CHEMICAL ENGINEERING ATTN M W BECKSTEAD PROVO UT 84058
1	CALIFORNIA INST OF TECH JET PROPULSION LAB ATTN L STRAND MS 233 103 4800 OAK GROVE DRIVE PASADENA CA 91109
1	CALIFORNIA INST OF TCHLGY ATTN F E C CULICK MC 301 46 204 KARMAN LAB PASADENA CA 91125
1	UNIV OF CALIFORNIA LOS ALAMOS SCIENTIFIC LAB P O BOX 1663 MAIL STOP B216 LOS ALAMOS NM 87545
1	UNIV OF CA BERKELEY CHEMISTRY DEPARMENT ATTN C BRADLEY MOORE 211 LEWIS HALL BERKELEY CA 94720
1	UNIV OF CA SAN DIEGO ATTN F A WILLIAMS AMES B010 LA JOLLA CA 92093

NO. OF COPIES	ORGANIZATION	NO. OF COPIES	ORGANIZATION
2	UNIV OF CA SANTA BARBARA QUANTUM INST ATTN K SCHOFIELD M STEINBERG SANTA BARBARA CA 93106	1	THE JOHNS HOPKINS UNIV CPIA ATTN T W CHRISTIAN 10630 LITTLE PATUXENT PKWY SUITE 202 COLUMBIA MD 21044-3200
1	UNIV OF COLORADO AT BOULDER ENGINEERING CTR ATTN J DAILY CAMPUS BOX 427 BOULDER CO 80309-0427	1	UNIV OF MICHIGAN GAS DYNAMICS LAB ATTN G M FAETH AEROSPACE ENGNRNG BLDG ANN ARBOR MI 48109-2140
3	UNIV OF SOUTHERN CA DEPT OF CHEMISTRY ATTN R BEAUDET S BENSON C WITTIG LOS ANGELES CA 90007	1	UNIV OF MINNESOTA DEPT OF MECHNCL ENGNRNG ATTN E FLETCHER MINNEAPOLIS MN 55455
1	CORNELL UNIV DEPT OF CHEMISTRY ATTN T A COOL BAKER LAB ITHACA NY 14853	4	PENNSYLVANIA STATE UNIV DEPT OF MECHNCL ENGNRNG ATTN K KUO M MICCI S THYNELL V YANG UNIVERSITY PARK PA 16802
1	UNIV OF DELAWARE CHEMISTRY DEPT ATTN T BRILL NEWARK DE 19711	2	PRINCETON UNIV FORRESTAL CAMPUS LIB ATTN K BREZINSKY I GLASSMAN P O BOX 710 PRINCETON NJ 08540
1	UNIV OF FLORIDA DEPT OF CHEMISTRY ATTN J WINEFORDNER GAINESVILLE FL 32611	1	PURDUE UNIV SCHL OF AERO & ASTRO ATTN J R OSBORN GRISSOM HALL WEST LAFAYETTE IN 47906
3	GEORGIA INST OF TECHLGY SCHOOL OF AEROSPACE ENGINEERING ATTN E PRICE W C STRAHLE B T ZINN ATLANTA GA 30332	1	PURDUE UNIV DEPT OF CHEMISTRY ATTN E GRANT WEST LAFAYETTE IN 47906
1	UNIV OF ILLINOIS DEPT OF MECH ENG ATTN H KRIER 144MEB 1206 W GREEN ST URBANA IL 61801	2	PURDUE UNIV SCHL OF MECHANICAL ENGNRNG ATTN N M LAURENDEAU S N B MURTHY TSPC CHAFFEE HALL WEST LAFAYETTE IN 47906

NO. OF COPIES	ORGANIZATION	NO. OF COPIES	ORGANIZATION
1	RENSSELAER POLYTCHNC INST DEPT OF CHEMICAL ENGNRG ATTN A FONTIJN TROY NY 12181	1	GENERAL APPLIED SCIENCE LABS INC 77 RAYNOR AVE RONKONKAMA NY 11779-6649
1	STANFORD UNIV DEPT OF MECHNCL ENGNRNG ATTN R HANSON STANFORD CA 94305	1	GENERAL ELECTRIC ORDNANCE SYSTEMS ATTN J MANDZY 100 PLASTICS AVE PITTSFIELD MA 01203
1	UNIV OF TEXAS DEPT OF CHEMISTRY ATTN W GARDINER AUSTIN TX 78712	1	GENERAL MOTORS RSCH LABS PHYSICAL CHEMISTRY DEPT ATTN T SLOANE WARREN MI 48090-9055
1	VA POLYTECH INST AND STATE UNIV ATTN J A SCHETZ BLACKSBURG VA 24061	2	HERCULES INC ATTN W B WALKUP E A YOUNT P O BOX 210
1	APPLIED COMBSTN TECHLGY ATTN A M VARNEY P O BOX 607885 ORLANDO FL 32860	1	ROCKET CTR WV 26726 HERCULES INC ATTN R V CARTWRIGHT 100 HOWARD BLVD
2	APPLIED MECHANICS REVIEWS ASME ATTN R WHITE & A WENZEL 345 E 47TH ST NEW YORK NY 10017	1	KENVIL NJ 07847 ALLIANT TECHSYSTEMS INC ATTN R E TOMPKINS MN 11 2720 600 SECOND ST NORTH
1	TEXTRON DEFENSE SYSTEMS ATTN A PATRICK 2385 REVERE BEACH PKWY EVERETT MA 02149-5900	1	HOPKINS MN 55343 IBM CORPORATION RESEARCH DIVISION
1	BATTELLE TWSTIAC 505 KING AVE COLUMBUS OH 43201-2693	1	ATTN A C TAM 5600 COTTLE RD SAN JOSE CA 95193 IIT RESEARCH INST
1	COHEN PROFESSIONAL SVCS ATTN N S COHEN 141 CHANNING ST REDLANDS CA 92373	1	ATTN R F REMALY 10 WEST 35TH ST CHICAGO IL 60616 LOCKHEED MIS & SPACE CO
1	EXXON RESEARCH & ENG CO ATTN A DEAN ROUTE 22E ANNANDALE NJ 08801		ATTN GEORGE LO 3251 HANOVER ST DEPT 52 35 B204 2 PALO ALTO CA 94304

NO. OF COPIES	ORGANIZATION	NO. OF COPIES	ORGANIZATION
1	OLIN ORDNANCE ATTN V MCDONALD LIB P O BOX 222 ST MARKS FL 32355-0222	3	THIOKOL CORPORATION WASATCH DIVISION ATTN S J BENNETT P O BOX 524 BRIGHAM CITY UT 84302
1	PAUL GOUGH ASSOCIATES INC ATTN P S GOUGH 1048 SOUTH ST PORTSMOUTH NH 03801-5423	1	UNITED TECHNOLOGIES RESEARCH CTR ATTN A C ECKBRETH EAST HARTFORD CT 06108
1	HUGHES AIRCRAFT CO ATTN T E WARD 8433 FALLBROOK AVE CANOGA PARK CA 91303	1	UNITED TECHNOLOGIES CORP CHEMICAL SYSTEMS DIV ATTN R R MILLER P O BOX 49028 SAN JOSE CA 95161-9028
1	SCIENCE APPLICATIONS INC ATTN R B EDELMAN 23146 CUMORAH CREST WOODLAND HILLS CA 91364	1	UNIVERSAL PROPULSION CO ATTN H J MCSPADDEN 25401 NORTH CENTRAL AVE PHOENIX AZ 85027-7837
3	SRI INTERNATIONAL ATTN G SMITH D CROSLEY D GOLDEN 333 RAVENSWOOD AVE MENLO PARK CA 94025	1	VERITAY TECHLGY INC ATTN E B FISHER 4845 MILLERSPORT HWY EAST AMHERST NY 14051-0305
1	STEVENS INST OF TECH DAVIDSON LAB ATTN R MCALEVY III HOBOKEN NJ 07030	1	FREEDMAN ASSOCIATES ATTN E FREEDMAN 2411 DIANA RD BALTIMORE MD 21209-1525
1	SVERDRUP TECHLGY INC LERC GROUP ATTN R J LOCKE MS SVR 2 2001 AEROSPACE PARKWAY BROOK PARK OH 44142	6	ALLIANT TECHSYSTEMS INC ATTN C CANDLAND L OSGOOD R BECKER J BODE R BURETTA M SWENSON 600 SECOND ST NE HOPKINS MN 55343
1	SVERDRUP TECHLGY INC ATTN J DEUR 2001 AEROSPACE PARKWAY BROOK PARK OH 44142	1	DIRECTOR US ARMY BENET LABS ATTN AMSTA AR CCB T SAM SOPOK WATERVLIET NY 12189
3	THIOKOL CORPORATION ELKTON DIVISION ATTN R BIDDLE R WILLER TECH LIB P O BOX 241 ELKTON MD 21921		

NO. OF
COPIES   ORGANIZATION

ABERDEEN PROVING GROUND

35   DIR USARL
         ATTN: AMSRL-WT-P, A HORST
                 AMSRL-WT-PC,
                   B E FORCH
                   G F ADAMS
                   W R ANDERSON
                   R A BEYER
                   S W BUNTE
                   C F CHABALOWSKI
                   K P MCNEILL-BOONSTOPPEL
                   A COHEN
                   R CUMPTON
                   R DANIEL
                   D DEVYNCK
                   N F FELL
                   J M HEIMERL
                   B HOMAN
                   A J KOTLAR
                   W F MCBRATNEY
                   K L MCNESBY
                   N E MEGHER
                   M S MILLER
                   A W MIZIOLEK
                   J B MORRIS
                   J E NEWBERRY
                   S A NEWTON
                   R A PESCE-RODRIGUEZ
                   B M RICE
                   L SEGER
                   P V SHARMILA
                   R C SAUSA
                   M A SCHROEDER
                   W TEAGUE
                   J A VANDERHOFF
                   D VENIZELOS
                   A WHREN
                   C WILLIAMSON

INTENTIONALLY LEFT BLANK.

USER EVALUATION SHEET/CHANGE OF ADDRESS

This Laboratory undertakes a continuing effort to improve the quality of the reports it publishes. Your comments/answers to the items/questions below will aid us in our efforts.

1. ARL Report Number/Author ___ARL-TR-1217 (Pai)___ Date of Report ___October 1996___

2. Date Report Received _____

3. Does this report satisfy a need? (Comment on purpose, related project, or other area of interest for which the report will be used.) _____

_____

_____

4. Specifically, how is the report being used? (Information source, design data, procedure, source of ideas, etc.) _____

_____

_____

5. Has the information in this report led to any quantitative savings as far as man-hours or dollars saved, operating costs avoided, or efficiencies achieved, etc? If so, please elaborate. _____

_____

_____

6. General Comments. What do you think should be changed to improve future reports? (Indicate changes to organization, technical content, format, etc.) _____

_____

_____

_____

CURRENT
ADDRESS

Organization

Name

Street or P.O. Box No.

City, State, Zip Code

7. If indicating a Change of Address or Address Correction, please provide the Current or Correct address above and the Old or Incorrect address below.

OLD
ADDRESS

Organization

Name

Street or P.O. Box No.

City, State, Zip Code

(Remove this sheet, fold as indicated, tape closed, and mail.)
(DO NOT STAPLE)

DEPARTMENT OF THE ARMY

OFFICIAL BUSINESS

<div style="border:2px solid black; display:inline-block; padding:4px;">

BUSINESS REPLY MAIL
FIRST CLASS PERMIT NO 0001, APG, MD

</div>

POSTAGE WILL BE PAID BY ADDRESSEE

DIRECTOR
US ARMY RESEARCH LABORATORY
ATTN AMSRL WT PC
ABERDEEN PROVING GROUND MD 21005-5066

NO POSTAGE
NECESSARY
IF MAILED
IN THE
UNITED STATES